UNIVERSIDAD POLITÉCNICA DE MADRID

ESCUELA TÉCNICA SUPERIOR DE INGENIEROS INDUSTRIALES

Assessment of SCALE capabilities for full core Monte Carlo burnup calculations of Sodium Fast Reactors

MASTER THESIS

Antonio Jiménez Carrascosa

BSc in Energy Engineering, Universidad de Málaga

2018

Master Thesis Director: **Dña. Nuria García Herranz**
Associate Professor of Nuclear Engineering
Universidad Politécnica de Madrid

This study has been prepared within EU Project ESFR-SMART which has received funding from the EURATOM Research and Training Programme 2014-2018 under Grant Agreement No 754501.

Acknowledgments

First of all, I would like to express my greatest appreciation to my MSc Thesis director, Dña. Nuria García Herranz. It is an enormous privilege to work with her.

I would also like to acknowledge workmates of Paul Scherrer Institute who are involved in the ESFR-SMART project for providing us with the SERPENT resources used in this MSc Thesis.

Last but not least, I would like to thank my family for their unconditional support.

En primer lugar me gustaría expresar mi mayor agradecimiento a mi directora de Trabajo Fin de Máster, Dña. Nuria García Herranz. Trabajar con ella es para mi todo un privilegio y nunca podré estar lo suficientemente agradecido por su confianza.

No puedo dejar de agradecer a mis compañeros de Departamento su inestimable acogida y la ayuda que me han proporcionado.

Por último pero no menos importante, muchas gracias a mi familia por el apoyo que siempre me han mostrado.

Abstract

Sodium-cooled fast reactors (SFR) have been identified as very promising technology within Generation IV of nuclear reactors. Taking into account the SFR capabilities and their operative experience, even as commercial operation, it may be expected that this technology plays an important role over future nuclear energy.

The SFR integration to nuclear fuel cycle would lead to an optimization of the natural resource use as well as to the nuclear waste reduction, making possible the operation using the spent and reprocessed fuel of current nuclear power plants. This fact has caused a recovery of the interest about this technology and several projects have been launched in order to demonstrate the SFR capabilities.

ASTRID is the European proposed prototype whose objective is to demonstrate the viability and reliability of sodium-cooled fast reactors. In close cooperation with the ASTRID program and as next step, the ESFR-SMART project was launched in 2017 having as final goal the ESFR (*European Sodium Fast Reactor*) development. The project's objective is to enhance the SFR safety measures as well as their detailed assessment. For this purpose, well-calibrated and validated computational tools are required in order to study the impact of the implemented safety measures over the reactor core physics.

Within the framework of the ESFR-SMART project, and with the objective of assessing and improving computational tools for fast reactor neutronics calculations, this MSc Thesis originates. The main goal of this work is to assess the SCALE Code System capabilities for full core Monte Carlo transport/depletion calculations with continuous energy treatment.

Depletion calculations are based on the coupling between neutron transport and inventory codes. Accuracy of the results depends, among others, on the code approximations and on the coupling method. In previous versions, SCALE Code System provided the capability to carry out burnup calculations based on the deterministic approximation (NEWT code) for neutron transport in a coupled way with the inventory code ORIGEN. In recent releases SCALE has built-in the Monte Carlo KENO code for neutron transport on burnup calculations, both in multigroup and continuous energy.

It is possible now to perform full core coupled KENO/ORIGEN calculations with SCALE. In this project, the applicability and limitations related to the use of this tool for

SFR analysis are evaluated. For this purpose, SCALE results are compared to the ones provided by Serpent code.

Firstly, a simplified 3-D pin-cell model is used in order to make an exhaustive analysis concerning multigroup applicability for fast spectrum and branching ratios and fission yields consideration. Likewise, an in-depth study of the differences between SCALE and Serpent will be performed by using this simplified model.

Secondly, a full core model for ASTRID-like reactor is used. Taking into account the model heterogeneity, it is of interest to assess the computational resources required for the whole coupled transport/depletion problem.

SCALE code, among others, will be applied to the ESFR design to be developed in the framework of ESFR-SMART project. Then, as a result of this MSc Thesis, it will be possible to know the SCALE limitations for once-through burnup calculations to be performed for the ESFR safety analysis.

Resumen

Dentro de los sistemas incluidos en la Generación IV de reactores nucleares, los reactores rápidos de sodio (SFR) han sido identificados como una de las opciones más prometedoras. Dadas sus capacidades y la experiencia operativa que se tiene de ellos, incluso a nivel comercial, cabría esperar que esta tecnología tuviese un papel importante en la energía nuclear del futuro.

La integración de los SFR al ciclo de combustible nuclear llevaría a una optimización en el uso del recurso natural así como a una reducción del residuo nuclear, pudiendo emplear incluso el combustible gastado y reprocesado de las actuales centrales nucleares. Esto ha provocado un repunte en el interés por esta tecnología, proponiéndose distintos proyectos con el objetivo de demostrar las capacidades de la misma.

A nivel europeo, ASTRID es el prototipo planteado actualmente con el que se pretende demostrar la viabilidad y fiabilidad de los SFR. En estrecha colaboración con el programa ASTRID y como paso siguiente surge el proyecto ESFR-SMART, cuya meta final es el desarrollo del reactor europeo ESFR (*European Sodium Fast Reactor*). Dicho proyecto tiene como objetivo la mejora de las medidas de seguridad así como una evaluación detallada de las mismas. Para esto, se requieren herramientas computacionales correctamente validadas y calibradas que permitan un exhaustivo estudio de la física del reactor así como de las medidas de seguridad implementadas.

Dentro del marco del proyecto ESFR-SMART, el Trabajo Fin de Máster que se presenta a continuación tiene como objetivo la evaluación y la mejora de las herramientas computacionales en su aplicación a la neutrónica de reactores rápidos. El principal objetivo de este trabajo es la evaluación de las capacidades del sistema de códigos SCALE para cálculos de quemado a nivel de núcleo completo y en energía continua.

Los cálculos de quemado se llevan a cabo acoplando el código de transporte neutrónico con el código de inventario. La precisión de los resultados obtenidos dependerá, entre otras muchas cosas, de las aproximaciones implícitas en los propios códigos y del método de acoplamiento. En versiones previas, el sistema de códigos SCALE permitía realizar este tipo de cálculos utilizando la aproximación determinista para el transporte neutrónico de manera acoplada al código de inventario ORIGEN. En las últimas versiones ha incorporado además la opción de realizar el cálculo de quemado basando el transporte neutrónico en el código de Monte Carlo KENO, tanto en su versión en multigrupos como en energía

continua.

Ahora es posible llevar a cabo cálculos a nivel de núcleo completo basados en el sistema acoplado KENO/ORIGEN. Con este objetivo, en el trabajo que se presenta se evaluará tanto la aplicabilidad como las limitaciones asociadas al uso de SCALE para análisis de SFR.

En primer lugar, se empleará un modelo simplificado de pin-cell para estudiar el comportamiento del cálculo en multigrupos y la consideración de *branching ratios* y *fission yields* que SCALE emplea. Utilizando este modelo simplificado, se llevará a cabo un exhaustivo análisis de las diferencias entre SCALE y Serpent.

Seguidamente, el estudio se ampliará al cálculo de núcleo completo, para lo que se utilizará el modelo de ASTRID. Teniendo en cuenta la heterogeneidad del mismo se hace necesario analizar los recursos computacionales que se van a requerir para este cálculo.

SCALE, entre otros códigos, será aplicado al diseño de ESFR que ha de desarrollarse en el proyecto ESFR-SMART. Por lo tanto, como resultado de este trabajo, será posible conocer qué limitaciones presenta el código para el cálculo de quemado que ha de realizarse en el estudio de seguridad del ESFR.

Contents

List of Figures

List of Tables

List of Acronyms

ALFRED	Advanced Lead Fast Reactor European Demonstrator
ASTRID	Advanced Sodium Technological Reactor for Industrial Demonstration
BOL	Beginning of Life
CEA	French Alternative Energies and Atomic Energy Commission
CP-ESFR	Collaborative Project for an European Sodium Fast Reactor
GIF	Generation IV International Forum
CE	Continuous Energy
EOC	End of Cycle
ESFR-SMART	European Sodium Fast Reactor-Safety Measures Assessment and Research Tools
ESNII	European Sustainable Nuclear Industrial Initiative
LANL	Los Alamos National Laboratory
LWR	Light Water Reactor
MG	Multi Group
MYRRHA	Multi-purpose Hybrid Research Reactor for High-tech Applications
OECD	Organisation for Economic Co-operation and Development
ORNL	Oak Ridge National Laboratory
PSI	Paul Scherrer Institut
SCALE	Standardized Computer Analyses for Licensing Evaluation
SET Plan	European Strategic Energy Technology Plan
SFR	Sodium-cooled Fast Reactor
SNE-TP	Sustainable Nuclear Energy Technology Platform
UPM	Universidad Politécnica de Madrid
URR	Unresolved Resonance Range

Chapter 1

Introduction

1.1 Motivation

Nowadays, it is clear that society has to confront many challenges within the energy supply sector. A growing energy demand around the world, climate change and resource limitations generate a very complex framework. The necessity of massive electrical energy sources is evident but they have to be competitive economically and have minimal carbon emissions. At this point, nuclear energy is presented as potential future option but it has particular problems to solve.

Long-lived radioactive waste, safety aspects and nuclear proliferation are the main issues that nuclear energy has to deal. In addition, public opinion plays an important role in nuclear energy development, therefore it is necessary to demonstrate that the new reactors are safer than traditional reactors.

Taking into account these issues, Generation IV International Forum (GIF) was created in 2000, defining the four goals areas to advance nuclear energy into its fourth generation: sustainability, safety and reliability, economics and proliferation resistance [27].

GIF is the organization that coordinates Generation IV development and selected in 2002 the following six concepts:

- Gas-cooled Fast Reactor (GFR),
- Lead-cooled Fast Reactor (LFR),
- Molten Salt Reactor (MSR),
- Sodium-cooled Fast Reactor (SFR),
- Supercritical-water-cooled reactor (SCWR),
- Very-high-temperature reactor (VHTR).

All of them have to pass different phases within their development but there are some concepts that started with some advantage the race to commercial operation. This is the case of Sodium Fast Reactors and specifically, in Europe, taking into account the operational experience, the European Sustainable Nuclear Industrial Initiative (ESNII) identified the SFR as the most mature technology for implementation.

ESNII is the initiative launched by Sustainable Nuclear Energy Technology Platform (SNETP) [3] in November 2010 and the Generation IV systems to be developed are addressed in its roadmap. In order to follow ESNII roadmap, projects such as ESNII+ were launched with orientation of preparing ESNII for Horizon 2020 [2]. SFR prototype called ASTRID and irradiation facility MYRRHA are the main systems of ESNII although ALFRED Lead-cooled Fast Reactor and ALLEGRO Gas-cooled Fast Reactor are also into the roadmap.

ESNII roadmap also foresees the R&D program for commercial fast nuclear reactors. European Sodium Fast Reactor (ESFR) of large power (3600 MWt) could be the candidate for the commercial operation in Europe within the ASTRID prototype line. The ESFR conceptual design was developed in the frame of the 7th Framework Program CP-ESFR project (2009-2013) [17].

Following the FP7 CP-ESFR project and in close cooperation with ASTRID program, the ESFR-SMART (European Sodium Fast Reactor - Safety Measures Assessment and Research Tools) project was launched in 2017 with the objective to enhance the safety of SFR, particularly of the ESFR concept. Research centres, industries and universities collaborate within the project having as main objectives:

- Produce new experimental data to support calibration and validation of the computational tools,
- Test and qualify new instrumentation to support their utilization in the reactor protection systems,
- Perform further calibration and validation of the computational tools,
- Select, implement and assess new safety measures for the ESFR,
- Strengthen and link together new networks between the European sodium facilities and between European students working on the SFR projects.

The ESFR-SMART project, coordinated by Paul Scherrer Institut (PSI), is structured in twelve work packages (WP) grouped in three subprojects (SP) as shown in Figure 1.1. Subproject 1 is dedicated to analytical assessment of new safety measures for ESFR, including five WPs its goal is to produce a new ESFR concept. Subproject 2, which includes five WPs, is devoted to producing new data and instrumentation and codes validation. Management and interactions within the project are grouped in subproject 3, highlighting educational aspects and interactions between different project participants.

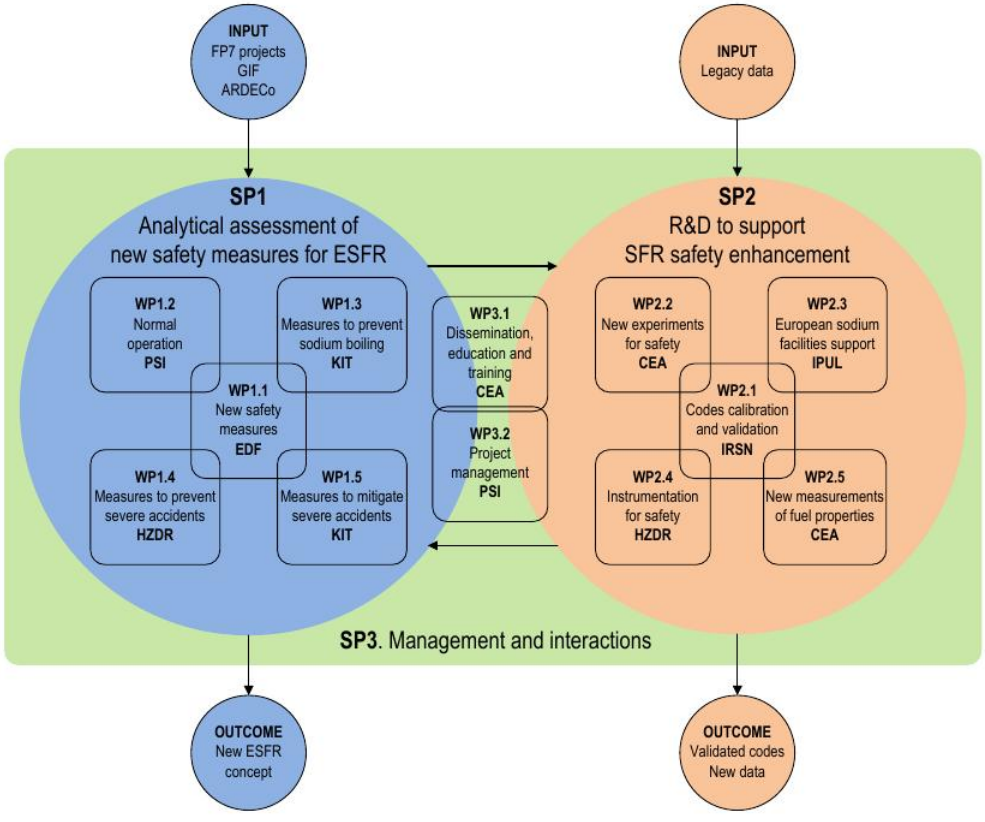

Figure 1.1: Organizational structure of the ESFR-SMART project [17].

Nineteen European partners (research institutes, companies and universities) are involved in ESFR-SMART project, being the Universidad Politécnica de Madrid (UPM) one of them. The UPM Research Group on Advanced Nuclear Fission Systems has large expertise in Sodium Fast Reactors. The group has participated, among others, in the European Projects of the 7th Framework Programme "European Sodium Fast Reactor (CP-ESFR)" [26, 16, 20] and "Preparing ESNII for HORIZON 2020 (ESNII+)" [5, 6, 19, 21]. In the framework of both projects, UPM contributed with core statics neutronics simulations to evaluate safety parameters together with the assessment of their uncertainties due to nuclear data in order to establish their confidence bounds.

Within ESFR-SMART project, UPM is involved, among others, in Task 1.2.1. "Initial core performance and burn-up calculations" in the framework of WP1.2. "Normal operation". Task 1.2.1. is dedicated to assessing the new reactor safety measures provided by WP1.1. "New safety measures". For this purpose, UPM will use SCALE code system [30], developed and managed by Oak Ridge National Laboratory (ORNL).

1.2 Objectives

SCALE provides a comprehensive tool set for criticality, reactor physics and sensitivity and uncertainty analysis. This tool has been used since 1980 by regulators, licensees and research institutions and it has been mainly validated and verified for thermal systems. Now, the main objective of this work is the assessment of SCALE code system capabilities for full core Monte Carlo transport-burnup coupled calculations of fast reactors.

The available SCALE tools to tackle that problem are: KENO (for Monte Carlo transport calculations) and ORIGEN (for depletion and decay calculations), both coupled through TRITON sequence. Those calculations can be carried out using continuous energy (CE) or multigroup (MG) libraries. Calculations in MG mode require shorter overall execution times for equivalent uncertainty than CE mode but MG libraries must be appropriated to preserve CE results. At present, the MG libraries distributed with SCALE are especially suitable for thermal systems, so it is compulsory to assess the MG libraries for fast reactor applications.

Therefore, the applicability of SCALE for full core transport-depletion of fast reactors has to be assessed, in both CE and MG modes, being the main goal of this MSc Thesis. It is expected to know SCALE limitations and assess the biases between CE and MG SCALE calculations and with respect to other codes used by other partners in the ESFR-SMART project, in particular with respect to Serpent code [25]. For that purpose, ASTRID whole-core model developed in [6] will be used applying necessary modifications. Calculations for new ESFR concept generated into the ESFR-SMART project will follow the same methodology.

1.3 Structure

This MSc Thesis is structured in the following way. Firstly, in Chapter 2, to establish a reference framework, main characteristics of Sodium Fast Reactors are briefly described, highlighting basic core physics aspects and main safety issues.

In Chapter 3, ASTRID specifications will be described in order to employ its full core model for the assessment of SCALE simulation tool.

Chapter 4 is dedicated to introduce transport-burnup coupling principles. Neutronics fundamental equations will be reviewed as well as approximations to solve them. Inventory and transport codes coupling will be described in this Chapter and also methodologies employed by tools used in this project: SCALE and Serpent.

Then, in Chapter 5 a transport-burnup calculation for an ASTRID pin-cell will be performed to assess SCALE capabilities for a simplified case.

The main section of this MSc Thesis is Chapter 6. Full core Monte Carlo transport-burnup calculations will be performed, including the following contents:

- SCALE multigroup calculations,
- SCALE continuous energy calculations,
- Serpent continuous energy calculations,
- Results comparison and conclusions extracted from calculations.

Finally, in Chapter 7, the main conclusions of the project will be presented as well as the possible future work.

Chapter 2

Sodium fast reactors

2.1 Introduction

As mentioned in Chapter 1, there are some designs into Generation-IV which have a relevant historical development. In the 1940s and the 1950s, fast neutron spectrum reactors were studied and experimented in a parallel way with thermal neutron reactors. In fact, the first power-generating nuclear reactor, called EBR-I and developed at Idaho National Laboratory (USA), was a liquid metal-cooled and fast neutron spectrum system[9].

Fast reactors presented, and present currently, some advantages related to resource utilization with respect to thermal neutron reactors. Then, several programs were launched in order to develop fast reactors, from experimental phase to commercial operation: United States, Russia, the United Kingdom, Germany and France were the countries which took the initiative in that process. Sodium-cooled fast reactor was the system with a major presence within these programs and, concretely, France acquired a key role. RAPSODIE, diverged in 1967, was the French prototype for this purpose, followed by PHENIX, available in 1973, whose operation was a success contributing widely to operational experience of SFRs in this country. Next step was Superphenix, the largest sodium-cooled fast reactor (1200 MWe) ever built and operated around the world. Its grid connection was in 1985 and its shut down in 1998 after a chaotic operation, including periods of administrative shutdowns.

In Europe, other projects were initiated and developed in Germany (KNK-II and SNR-300) and in United Kingdom (DFR and PFR). After Superphenix and as next step, a concept of the European Sodium Fast Reactor (EFR project) was born in 1990s but the project was stopped in late 90s. EFR project would make use of the operational experience extracted of Superphenix and established a wide European cooperation. New European projects such as FP7 CP-ESFR, in 2000s, were result of renewed interest in the Sodium Fast Reactors.

PHENIX, operational until 2009, was the last European sodium-cooled fast reactor

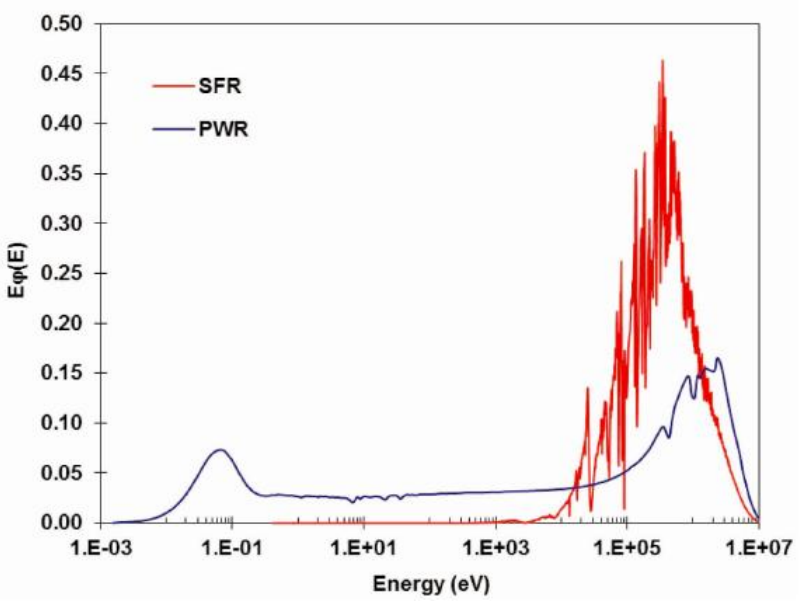

Figure 2.1: Typical neutron flux spectra of thermal and fast reactors [32].

but nowadays there are reactors of this type under operation (BN-800 in Russia and CEFR in China) or under construction (PFBR in India and CFR-600 in China). In fact, CFR-600 construction has begun recently -December 2017- and it will be the reference design for the future commercial-scale unit CFR-1000 whose construction should start in December 2028. It is evident that this technology will have an important role on the future of nuclear industry and it is clear into the Generation-IV Roadmap [27].

In the following sections, basic aspects related to core physics and safety of SFRs will be briefly presented in order to establish a consistent framework for the rest of the work. Taking into account this project thematic, the information will be focused on neutronics issues such as fast neutron spectrum characteristics.

2.2 Sodium fast reactor physics

It is well-known the moderation process that takes place into a thermal reactor where neutrons are slowed down from energies from MeV to eV. The principle of fast neutron reactor is to avoid this process and to operate with a fast neutron spectrum, centered into the keV to MeV range as it is showed in Figure 2.1.

To achieve fast neutron spectrum, moderation should be minimized by avoiding the use of low atomic mass nuclides. The light water, used in thermal reactors, induces large neutron energy losses by elastic scattering and because of that it is necessary the use of alternative coolants. These coolants have to present a low scattering cross section in

addition to adequate thermal properties. Liquid metals and gas coolants are being studied as coolants for fast reactors, highlighting the liquid sodium.

Liquid sodium presents interesting neutronic characteristics:

- A very low neutron moderating power,
- Little neutron capturing power,
- Low level of activation under irradiation.

Therefore, sodium is transparent enough to neutrons allowing the operation with fast neutron spectrum. Nevertheless, sodium presents some disadvantages related to chemical and physical properties; strongly sodium-water reaction or chemical affinity with oxygen.

To operate with a fast neutron spectrum supposes a significant change on the reactor physics with respect to thermal reactors due to the energy dependence of the reaction cross sections. Consequently, fast reactors present some advantages such as optimized use of fuel resources and the actinide transmutation capability. These advantages and main reactivity feedback coefficients are detailed in the following subsections.

2.2.1 Breeding and resource utilization

Fast reactors present a high flexibility in managing materials and it would be possible to operate the reactors in a breeder mode. In this case, the reactor generates more fissile material than is consumed by converting fertile materials into fissile ones. The most interesting breeding chain starts from U-238 and finishes with Pu-239 production:

$$U^{238}(n,\gamma)U^{239} \longrightarrow Np^{239} \longrightarrow Pu^{239}$$

This chain is presented as the most interesting in order to direct natural uranium utilization as nuclear fuel. However, a sufficient supply of neutrons must be ensured to maintain the reaction. The necessary condition for breeding is $\eta > 2$ [15], defining η as:

$$\eta = \frac{\nu\sigma_f}{\sigma_a} \tag{2.1}$$

Where ν is the number of neutrons produced per fission, σ_f is the fission cross section and σ_a as absorption cross section. Therefore, η represents the number of neutrons produced per neutron absorbed. This parameter has to be greater than 2 because a neutron is required to sustain the nuclear chain reaction, one neutron is necessary to ensure the transmutation of U-238 to Pu-239 and leaks have to be compensated. The values of η for U-235 and Pu-239 are represented in Figure 2.2.

Figure 2.2 shows that Pu-239 used in a fast reactor makes possible the utilization of natural uranium as nuclear fuel. A plutonium and natural uranium based fuel will be

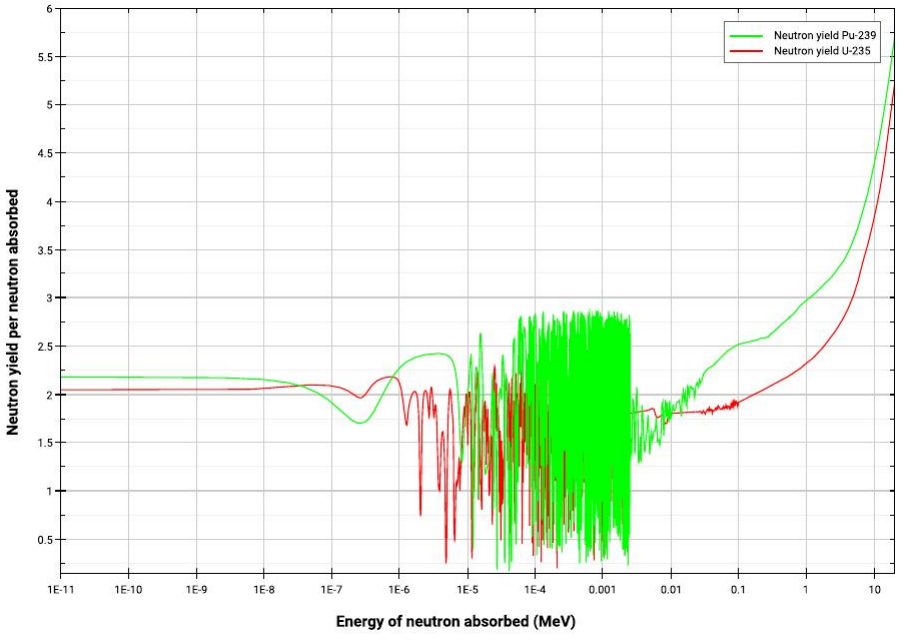

Figure 2.2: Neutron yield per neutron absorbed for U-235 and Pu-239 obtained by ENDF/B-VII.1 nuclear data library.

the main option for the fissile material of fast reactors. Typically, a fertile material called blanket will surround the fissile material into the core, which main objectives are the production of new fissile material or minor actinides transmutation.

These properties are presented as promising in order to achieve an optimized resource utilization. It would be possible to use directly natural uranium or depleted uranium which results from enrichment tails of LWR fuel fabrication.

2.2.2 Minor actinide transmutation

Another advantage related to core physics of fast reactors is the possibility to transmutate some minor actinides (Am, Cm or Np). Transmutation principle consists in modifying the nuclei of long-lived elements by neutron irradiation to obtain stable isotopes or shorted-lived ones [9].

Minor actinide transmutation capability is dominated by two types of nuclear reactions: neutron capture and nuclear fission. To have an efficient transmutation process depends on the competence between this two reactions. A capture reaction would generate other actinides while a fission reaction would cause the actinide destruction into two fragments. Thus, a high fission-to-capture ratio would be desired to achieve the objective. Taking into account the energy dependence of the reaction cross sections, a variation of the defined ratio between thermal and fast spectrum will be expected. Table 2.1 shows

Isotopes	Thermal Reactor	Fast Reactor
Np-237	0.0333	0.1887
Am-241	0.0225	0.1351
Am-243	0.0158	0.1163
Cm-244	0.0763	0.7143
Cm-245	5.0	5.5556

Table 2.1: Typical fission-to-capture ratios (σ_f/σ_c) for thermal and fast reactors [9].

fission-to-capture ratio for some minor actinide isotopes.

As can be seen in Table 2.1, in fast reactors, the ratio is increased by a factor of 5 to 10 compared to thermal reactors. Then, operation with fast neutron spectrum will allow a more efficient minor actinides transmutation by direct fission with less generation of higher actinides. Cm-245 ratio is similar in thermal and fast reactors with fission reaction domination, hence it will be transmuted by both systems in a similar way.

Minor actinide elimination is presented as very promising option to nuclear waste management. These isotopes are the main contributors to the high long-term radiotoxicity of nuclear waste, therefore their elimination would enable a lower waste storage time.

2.2.3 Reactivity feedback coefficients

Related to core physics, reactivity feedback coefficients play a key role in the safety assessment under external perturbations. Total reactivity feedback during a normal or incident operating transient has to lead in the recovery of whole-core equilibrium state. This is a common characteristic for LWR and SFR where temperature changes of different materials can result in the variation of multiplication factor (k_{eff}).

In SFR, these coefficients can be gathered into three main groups:

- Doppler effect, induced by fuel temperature changes and consequently related to the variation in the resonant absorption of the nuclei occurring in fuel.
- Sodium-related effects such as the sodium void effect and coolant expansion. When sodium is partly or fully removed, three processes are induced: an increase of neutron leakage, an increase of absorptions in the fuel and the hardening of neutron spectrum [26]. The first process leads to a negative effect on the reactivity but another two induce a positive reactivity insertion.
- Geometrical variation effects, dominated mainly by material thermal expansions which affect the geometry and the density of the materials and consequently the reactivity.

The assessment of reactivity feedback coefficients is essential in SFR safety analysis and they have an important impact into adopted core design.

2.3 Future prospects for SFRs

In Section 2.1, a brief review of Sodium Fast Reactors history has been presented but it will be interesting to describe the future prospects for this technology.

Nowadays, BN-800, the Russian 800 MWe sodium-cooled fast reactor is successfully operational and supposes an useful background to SFR development. However this technology requires significant advances; it is necessary to proof transmutation capabilities as well as related safety aspects. Aiming to demonstrate industrial viability and economical competitiveness of SFRs, France launched the ASTRID program in 2006.

ASTRID prototype (1500 MWth) has to demonstrate the operation as plutonium burner or as a breeder reactor. Its integration in a closed fuel cycle has to be assessed, reducing decay heat and the long-term radiotoxic inventory of nuclear waste. Definitely, ASTRID will be the reference concept for future commercial-size ESFR, the European 3600 MWth sodium-cooled fast reactor. It is expected that ASTRID prototype begins its operation before 2025.

In this line and following the FP7 CP-ESFR project, the ESFR-SMART project [1] will establish a novel concept of the large-power ESFR featuring enhanced safety level. Using the CP-ESFR legacy, the project will select new safety measures and their impact will be assessed on the ESFR defence-in-depth levels. The final goal is to produce an optimized ESFR design with an higher level of safety compared to traditional LWRs and SFRs in order to achieve a more reliable operation fulfilling all Generation-IV objectives.

It is important not to forget that the most part of all nuclear reactors operative today around the world are based in LWR technology. In this sense, a complementary operation between LWRs and fast reactors would be expected in the next years improving the nuclear fuel cycle sustainability.

Fast reactors can use the plutonium generated by water reactors without any restriction avoiding the treatment of plutonium as long-lived waste. Moreover, the possibility to transmute minor actinides makes achievable an optimized fuel cycle with a lower waste storage time. Therefore, fast reactors are presented as ideal complement to currently LWRs.

Chapter 3

ASTRID core specifications

3.1 Introduction

As mentioned in Section 1.2, ASTRID-like 1500 MWth oxide-fueled core is assumed as the reference model to assess the capabilities of SCALE for Monte Carlo burnup calculations. For this purpose, a brief review of ASTRID core specifications is presented in Section 3.2. Core geometry, fuel composition and material temperatures at nominal conditions are summarized throughout this Chapter.

Moreover, details related to models developed using SCALE and Serpent simulation tools are presented in Sections 3.3 and 3.4 respectively.

3.2 Specifications

ASTRID core geometry, materials and composition were defined within ESNII+ project framework and concretely issued in Deliverable D6.1.1-1 [31].

ASTRID is a medium-size (1500 MWth) design with two different fuel regions, the inner zone (IZ) and the outer zone (OZ). There is a radial reflector surrounding the outer zone and a radial shielding in the core external zone. Figure 3.1 shows the core radial layout.

As it can be seen, the inner zone is composed by 177 hexagonal sub-assemblies where UO_2-PuO_2 mixed fuel (MOX) is included as fissile material. On the other hand, the outer zone includes 114 sub-assemblies with a lower PuO_2 enrichment in the fissile material. At Beginning of Life (BOL), mass Pu enrichment in the inner fuel is 24.3%, while in the outer fuel the enrichment is 20.7%. Detailed fuel compositions at BOL are given in Table 3.1. Both zones incorporate fertile fuel regions based in UO_2 fertile material, the lower blanket (LB) and the inner blanket (IB). Inner and outer zone sub-assemblies present a triangular arrangement of 217 pins with AIM1 steel as cladding material. Moreover, fuel sub-assemblies are surrounded by the wrapper, an EM10 steel based hexagonal structure.

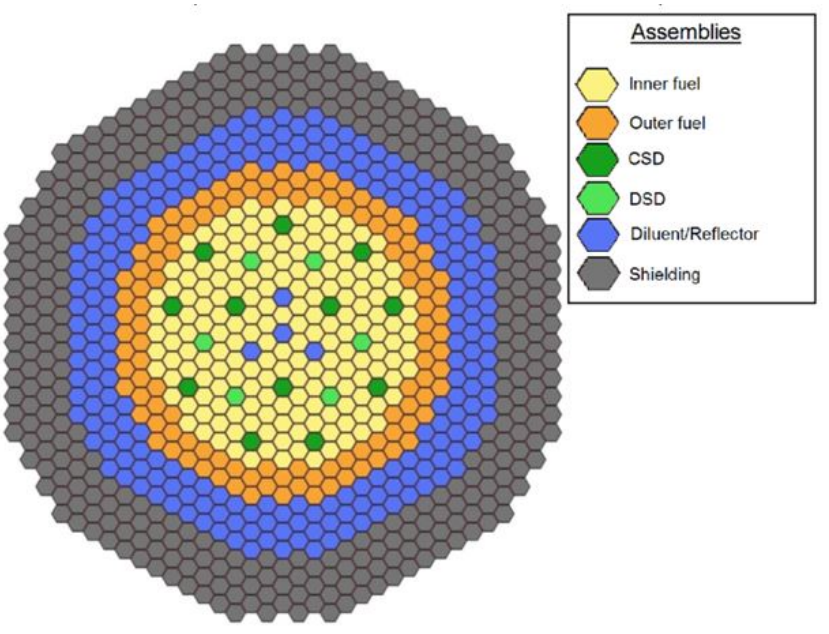

Figure 3.1: ASTRID core radial layout [19].

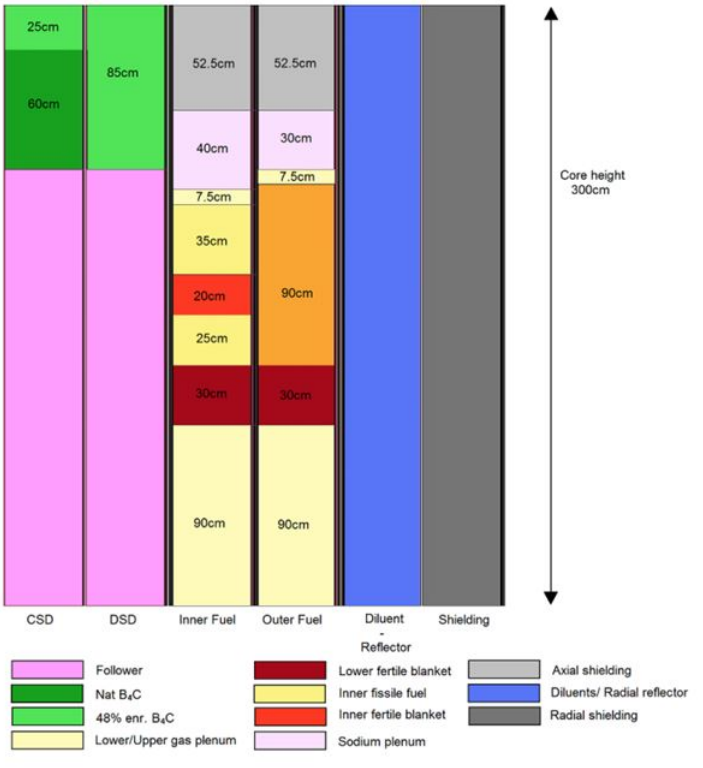

Figure 3.2: ASTRID core axial layout [19].

w/o	MOX-IZ	MOX-OZ	UO_2-IB	UO_2-LB
O-16	11.725%	11.727%	11.847%	11.847%
U-235	0.134%	0.140%	0.176%	0.176%
U-238	66.678%	69.849%	87.977%	87.977%
Pu-238	0.556%	0.474%	-	-
Pu-239	11.848%	10.093%	-	-
Pu-240	5.548%	4.726%	-	-
Pu-241	1.560%	1.329%	-	-
Pu-242	1.689%	1.439%	-	-
Am-241	0.262%	0.223%	-	-

Table 3.1: Beginning of life fuel composition in weight percent.

Radial reflector and radial neutron shielding are composed by 216 and 354 sub-assemblies respectively. Regulation, compensation and safety are handled by 12 CSD (Control and Shut-down Device) sub-assemblies and 6 DSD (Diverse Shut-down Device) sub-assemblies, all based on B_4C as absorbing material. These control rods are distributed within the inner zone as can be observed in Figure 3.1. At the center of the core 4 steel diluent sub-assemblies, whose composition is similar than radial reflector assemblies, are inserted.

The design presents an important axial heterogeneity (see Figure 3.2) with a fertile blanket common to inner and outer zone at the bottom of active core, the lower blanket mentioned previously. Moreover, an inner fertile zone called inner blanket is included within the inner zone between the lower and upper fissile zones.

As analysed by [5], axial heterogeneity presented in ASTRID core design leads to achieve a low sodium void effect, enhancing core safety compared to past SFR designs. An absorbing shielding on the top is included in order to prevent neutrons from going back to the core during voiding scenarios, a sodium plenum above the active core would maximize neutron leakage and a fertile blanket at the bottom of the core would increase the flux level at the upper surface. These features result in a reduced active core height with respect to the radial width.

Material temperatures at nominal conditions are given in Table 3.2. These temperatures have a direct influence over material expansion and atomic densities and, of course, over cross sections selected by the simulation tool.

Parameter	Temperature
Core average fissile fuel temperature	1500K
Core average fertile fuel temperature	900K
Core average cladding temperature	748K
Core average coolant temperature	748K
Core average wrapper assembly temperature	748K
Outlet coolant temperature (top sodium plenum)	823K

Table 3.2: Material temperatures at nominal conditions [31].

3.3 SCALE/TRITON model

ASTRID full core model was developed by [6] in order to be used by the SCALE 3-D Monte Carlo code, called KENO-VI, in the framework of the ESNII+ project. An exhaustive core performance analysis was carried out for End of Cycle (EOC) conditions, including reactivity coefficients, power distributions and control rod worth calculations.

Related to materials temperatures (Table 3.2), the work carried out by [6] presents some deviations between temperatures given by specifications and temperatures used by SCALE/KENO-VI for cross sections generation due to SCALE version used. SCALE version will be used in this project is able to generate problem-dependent cross sections by logarithmic interpolation, hence cross sections will be select for each material temperatures included in the input.

Model generated for KENO-VI will be applicable to coupled transport-burnup calculations by TRITON, the multipurpose SCALE control module for transport, depletion and sensitivity and uncertainty analysis [30]. Material compositions are adjusted to beginning of life conditions and TRITON particular blocks are included in the input. Depletion methodology followed by TRITON and required parameters will be described in Section 4.3.

The full core model will be used preserves radial and axial heterogeneities. Thus, high computational resources will be required in order to obtain the most accurate results as possible.

Figures 3.3 and 3.4 show radial and axial layouts of the 3-D full core model will be used by TRITON.

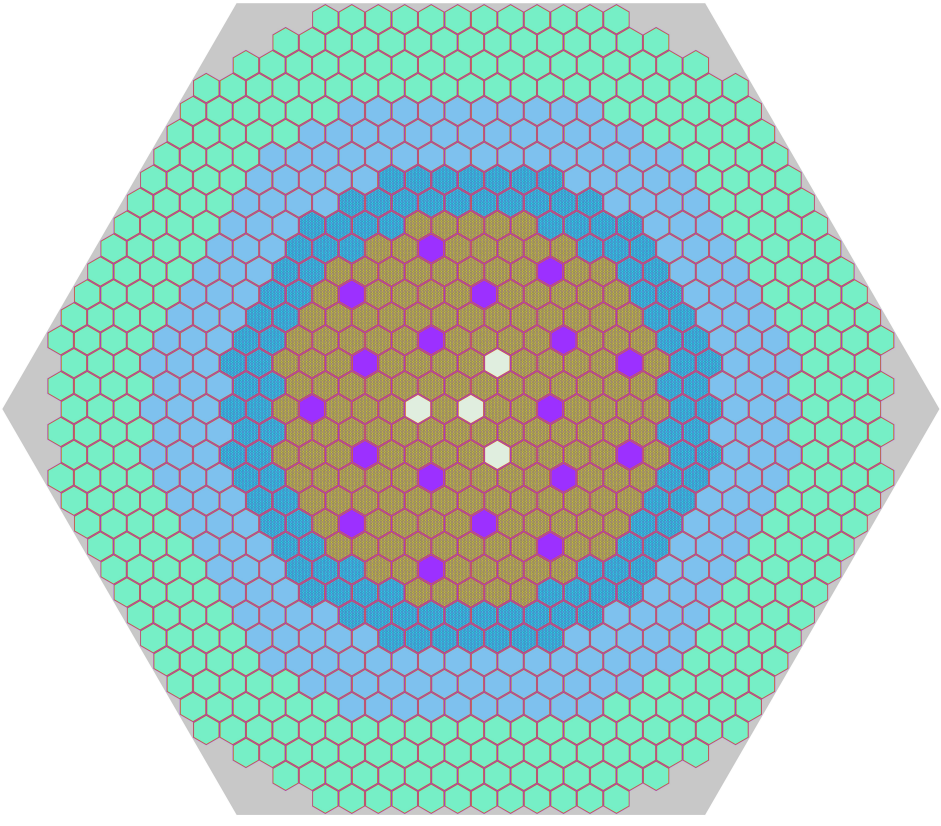

Figure 3.3: Radial layout of the 3-D core model in SCALE/TRITON [6].

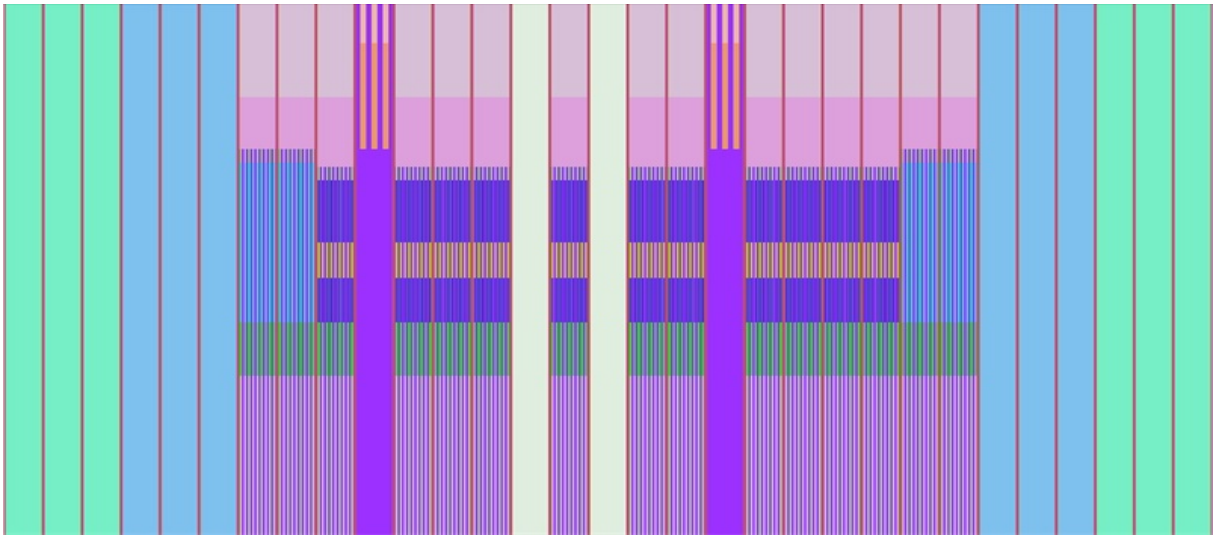

Figure 3.4: Axial layout of the 3-D core model in SCALE/TRITON [6].

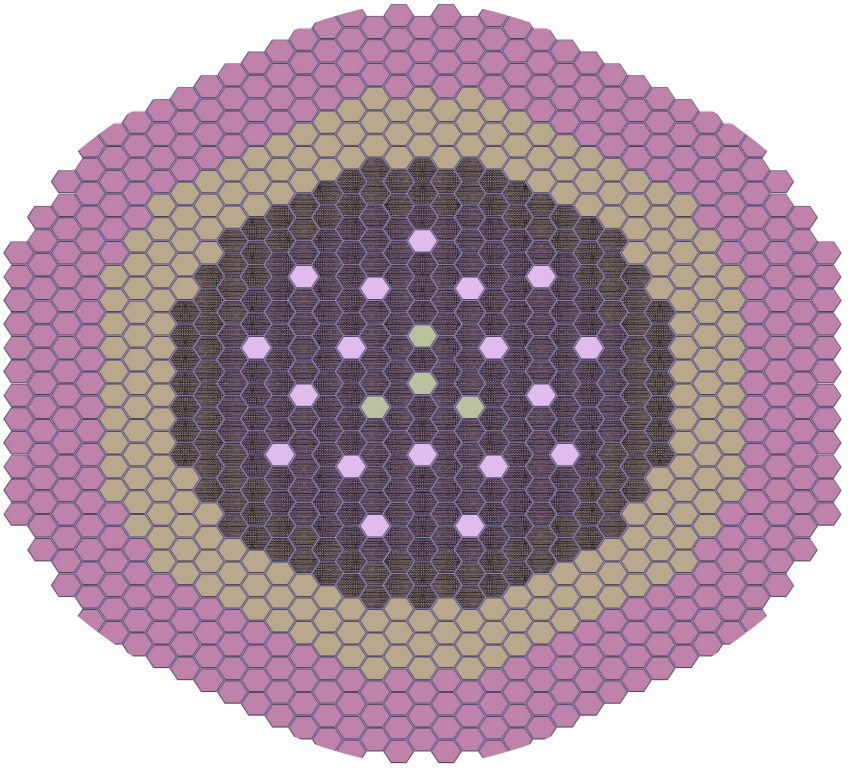

Figure 3.5: Radial layout of the 3-D core model in Serpent.

3.4 Serpent model

On the other hand, ASTRID model for Serpent code was developed by Paul Scherrer Institut (PSI) in the ESNII+ project framework. In a similar way than KENO-VI model, the input was generated for EOC conditions, then modifications are required in order to have the same geometry and material compositions.

Serpent incorporates a different methodology for transport-burnup coupled calculations compared to SCALE/TRITON. A detailed description of this methodology is included in Section 4.4.

Likewise, Figures 3.5 and 3.6 show radial and axial layouts of the 3-D full core model will be used by Serpent. As it can be seen, the model includes a fully resolved representation of different sub-assemblies preserving the axial heterogeneity.

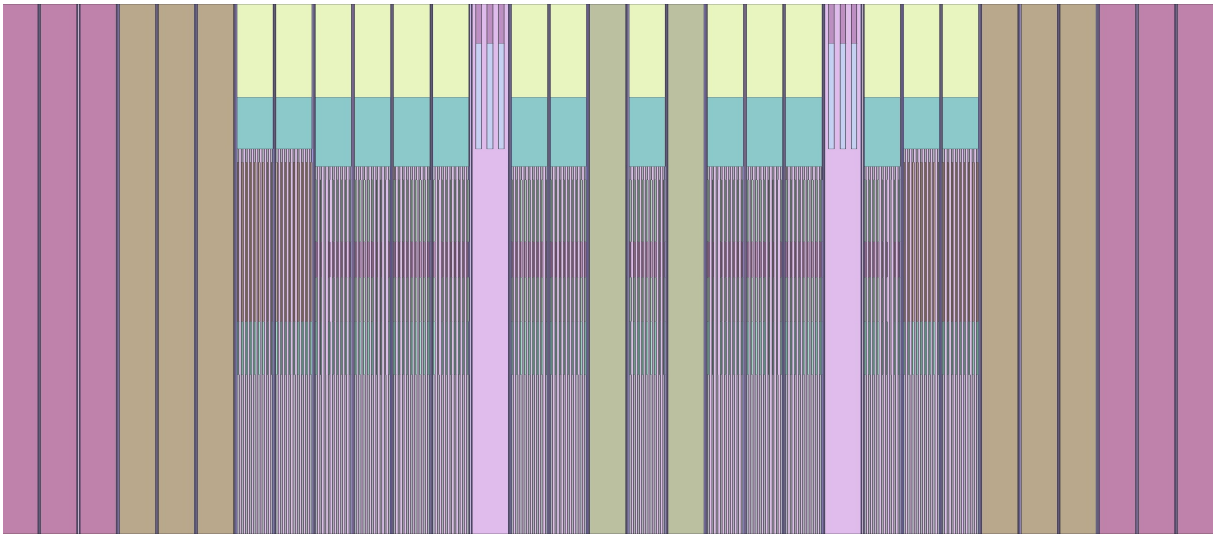

Figure 3.6: Axial layout of the 3-D core model in Serpent.

Chapter 4

Coupled transport-burnup calculations

4.1 Introduction

In this Chapter, the principles of coupled transport-burnup calculations are presented. Firstly, in Section 4.2, a brief summary of neutronic fundamental equations is presented in order to put the attention into the transport-burnup coupling. The dependence between transport and depletion equations is justified and theoretical approximation to their coupling is carried out.

Then, methodologies for coupled transport-burnup calculations followed by the simulation tools used in this project are analyzed. In Section 4.3, methodology followed by SCALE is presented, with a brief presentation of the code and main parameters required in the input. In a similar way, in Section 4.4, methodology implemented in Serpent is described, highlighting the main differences with SCALE code: the predictor-corrector algorithm and Bateman equations resolution methods.

Serpent is a widely-used simulation tool and it is capable of performing burnup calculations in a reliable way. Then, it will be the reference code for assessing the SCALE performance in this type of calculations.

4.2 Neutronics and transport-burnup coupling

Neutronics equations characterize neutron transport through matter and the changes that neutrons induce by nuclear processes. Neutron propagation is associated with the transmutation of the media in which they travel. Two main equations govern the system behaviour; the first one governs the neutron motion as a function of time and space and the other one the evolution of isotopic compositions [8]. These equations and their coupling are described in the following subsections.

4.2.1 Fundamentals of neutronics

In the core of a nuclear reactor, neutron behaviour is governed by the integro-differential Boltzmann equation, called neutron transport equation. The solution of the transport equation (Eq. 4.1) gives the neutron population's density as a function of time, energy and space.

$$\frac{1}{v}\frac{\partial\psi}{\partial t}(\bar{r},E,\bar{\Omega},t)+\bar{\Omega}\cdot\nabla\psi(\bar{r},E,\bar{\Omega},t)+\Sigma_t(\bar{r},E)\psi(\bar{r},E,\bar{\Omega},t)= \\ \frac{\chi(E)}{4\pi}\int_E\int_\Omega \nu\Sigma_f(\bar{r},E')\psi(\bar{r},E',\bar{\Omega}',t)d\Omega' dE' \\ +\int_E\int_\Omega \Sigma_s(\bar{r},E'\rightarrow E,\bar{\Omega}'\rightarrow\bar{\Omega})\psi(\bar{r},E',\bar{\Omega}',t)d\Omega' dE'+q(\bar{r},E,\bar{\Omega},t) \quad (4.1)$$

The transport equation represents the balance of neutron population in an elementary volume $D\equiv d\bar{r}\cdot dE\cdot d\bar{\Omega}$ around point $P\equiv(\bar{r},E,\bar{\Omega})$ of the phase space, during the elementary time interval dt around instant t. Thus, neutron's state is characterized by 7-dimensional phase space.

Typically, two main approximations, based in numerical methods, have been followed in order to solve the transport equation:

- Deterministic methods that provide the exact solution of the transport equation adopting model simplifications. These simplifications are related to discretization of the phase space: energy (multi groups), space and direction. Widely known simulation tools such as ERANOS (CEA, France) or PARCS (Purdue University, USA) are based on deterministic approaches.

- Stochastics or Monte Carlo methods, based on the individually study of neutrons behaviour. Simulating a large number of neutron histories it is possible to obtain the average statistical macroscopic behaviour of the system. Thus, Monte Carlo methods provide an approximate solution to real problem with a statistical error. These methods can be used for very complex geometries without simplifications, allowing continuous energy calculations which is of key importance for fast reactors [26]. In this sense, codes such as MCNP (LANL, USA), Serpent (VTT Technical Reasearch Centre, Finland) or KENO-VI, within SCALE code system (ORNL, USA), are presented as typical Monte Carlo simulation tools.

On the other hand, Bateman equation (Eq. 4.2) governs the time evolution in the concentration of the atomic nuclei taking into account nuclei generations and disappearances by nuclear reactions and radioactive decay process.

$$\frac{dN_k(\bar{r},t)}{dt} = \sum_{m\neq k} N_m(\bar{r},t)\sum_q \int_E \sigma_{q,k\leftarrow m}(E)\phi(\bar{r},E,t)dE + \sum_{m\neq k}\lambda_{k\leftarrow m}N_m(\bar{r},t) - \lambda_k N_k(\bar{r},t) - \sum_q \int_E \sigma_{q,k}(E)\phi(\bar{r},E,t)dE \cdot N_k(\bar{r},t) \quad (4.2)$$

Variation of nuclides k during irradiation is quantified as sources and sinks balance. Nuclear reactions from nuclides m to k and radioactive decay of nuclide m towards nuclide k are source terms. Sink terms correspond to radioactive decay of nuclide of type k and disappearance by nuclear reactions of nuclide k.

In a simplified way, Equation 4.2 could be expressed as Equation 4.3.

$$\dot{N}(\bar{r},t) = A(\bar{r},t)\cdot N(\bar{r},t) \quad (4.3)$$

Where $A(\bar{r},t)$ is defined as the matrix 4.4. Its coefficients are dependent on the neutronic flux $\phi(\bar{r},E,t)$ according to Equations 4.5 and 4.6.

$$A = \begin{bmatrix} a_{11} & a_{12} & \cdot & \cdot & a_{1n} \\ a_{21} & a_{22} & \cdot & \cdot & a_{2n} \\ \cdot & \cdot & \cdot & \cdot & \cdot \\ \cdot & \cdot & \cdot & \cdot & \cdot \\ a_{n1} & a_{n2} & \cdot & \cdot & a_{nn} \end{bmatrix} \quad (4.4)$$

$$a_{km} = \lambda_{k\leftarrow m} + \sigma_{k\leftarrow m}(E)\cdot\phi(\bar{r},E,t) \quad (4.5)$$

$$a_{kk} = -(\lambda_k + \sigma_k(E)\cdot\phi(\bar{r},E,t)) \quad (4.6)$$

Several computational tools for time evolution of radionuclide concentrations have been developed, highlighting CINDER (LANL, USA), FISPACT (UKAEA, UK), ORIGEN (ORNL, USA) and ACAB (UNED-UPM, Spain) as main inventory codes. These codes are able to solve the different transmutation chains dependent on neutronic flux distribution and working with activation products, actinides and fission products.

In summary, data required for solving the Boltzmann equation and main physical quantities deduced from it are summarized in Tables 4.1 and 4.2 respectively. In a similar way for Bateman equations, Tables 4.3 and 4.4 provide the main data required for solving the Bateman equations and the physical quantities deduced from them. As it can be deduced, neutron flux required to solve Bateman equation results by solving Boltzmann equation and concentration $N_k(\bar{r},t)$, that results by solving Bateman equations, is required for solving the Boltzmann equation. Then, it can be deduced that both equations constitute a coupled system.

Quantity	Notation
Concentration	$N_k(\bar{r}, t)$
Microscopic cross section	$\sigma(E)$
Macroscopic cross section	$\Sigma(\bar{r}, E, t) = N(\bar{r}, t) \cdot \sigma(E)$
Neutron multiplication by fission	ν
Fission spectrum	$\chi(E, E')$
External source	$q(\bar{r}, E, \bar{\Omega}, t)$

Table 4.1: Main data required for solving the Boltzmann neutron transport equation [8].

Quantity	Notation
Neutrons density	$n(\bar{r}, E, \bar{\Omega}, t)$
Angular flux	$\psi(\bar{r}, E, \bar{\Omega}, t) = n(\bar{r}, E, \bar{\Omega}, t) \cdot v$
Scalar flux	$\phi(\bar{r}, E, t)$
Total flux	$\phi(\bar{r}, t)$
Neutron current	$\bar{J}(\bar{r}, E, \bar{\Omega}, t) = \bar{\Omega} \cdot \psi(\bar{r}, E, \bar{\Omega}, t)$
Multiplication factor	k_{eff}
Reactivity	$\rho = \frac{k-1}{k}$

Table 4.2: Main physical quantities deduced from solving the Boltzmann equation [8].

Quantity	Notation
Partial decay constants	$\lambda_{\alpha,k},\ \lambda_{\beta^-,k}$,...
Energy-integrated microscopic reaction rates	$\int_E \sigma_{q,k\leftarrow m}(E)\phi(\bar{r}, E, t)dE$
Fission yields	$Y_{k\leftarrow f}(E)$

Table 4.3: Main data required for solving the Bateman equations [8].

Quantity	Notation
Concentration	$N_k(\bar{r}, t)$
Activity	$A_k(\bar{r}, t) = \lambda N_k(\bar{r}, t)$

Table 4.4: Physical quantities deduced from solving the Bateman equations [8].

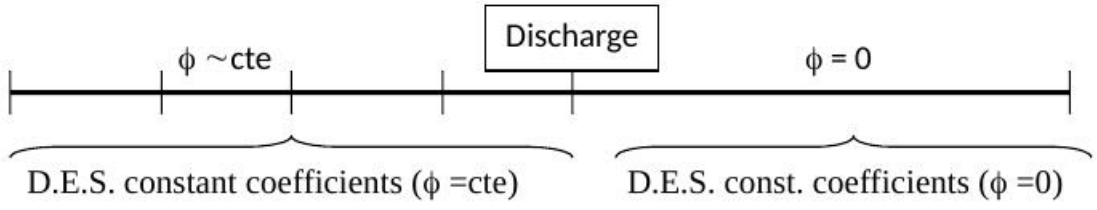

Figure 4.1: Simplified approximation to transport-burnup calculations.

4.2.2 Transport-burnup coupling

During nuclear reactor operation, radionuclide concentrations change as nuclear reactions occur. Isotopic variations will have an important influence over reactor parameters such as reactivity or power distribution, hence a methodology to solve transport and inventory equations in a coupled way is required.

Frequently, some simplifications are adopted assuming a constant neutronic flux and flux spectrum along irradiation time. This simplification derives in a differential equations system with constant coefficients which allows the problem approximation shown in Figure 4.1.

If the flux spectrum or total flux change significantly during irradiation time, it would not be reliable to assume a constant spectrum along the burnup time. To solve the inventory equation, the total neutronic flux is required and also the flux spectrum for calculation of the activation cross sections collapsed (Eq. 4.7) in the target group structure. Thus, a coupled resolution of transport and inventory equations is desirable, using the flux distribution provided by transport equation resolution in each burnup time step.

$$\sigma^{eff} = \frac{\sum_g \sigma^g \phi^g}{\sum_g \phi^g} \tag{4.7}$$

In this sense, Monte Carlo-based tools have been coupled with depletion codes in order to achieve more detailed burnup calculations. Monte Carlo codes present many advantages since make possible to treat complex geometries, very useful taking into account heterogeneities presented in a SFR whole-core model.

Codes such as MCNP-ACAB (UPM, Spain [18]), MONTEBURNS (LANL, USA) or EVOLCODE (CIEMAT, Spain) are some examples of computational tools which coupling a Monte Carlo transport code and a depletion code.

The most intuitive approximation to Monte Carlo burnup calculations is known as "beginning-of-step constant flux approximation". Full burnup time is divided into some time steps where the flux, at beginning of step, is assumed constant along the time step. Then, a transport calculation is carried out in order to determine the neutron flux at

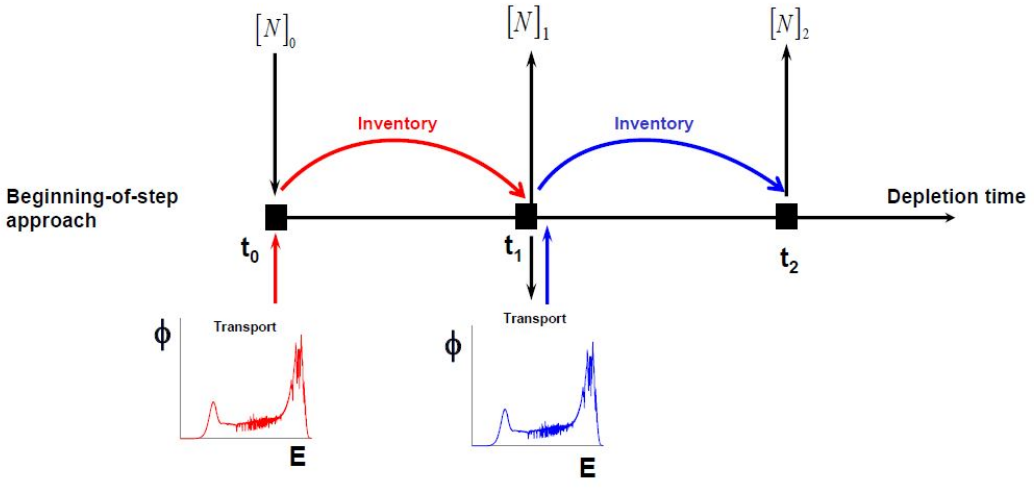

Figure 4.2: Beginning-of-step constant flux approximation to Monte Carlo burnup calculations.

beginning of step t_0. At end of step t_1, an inventory calculation is accomplished and a new transport calculation with updated isotopic concentrations is performed. Figure 4.2 shows the structure of this algorithm.

The tools will be used in this project, as which aforementioned, make possible the coupled resolution of transport and depletion equations. Methodology followed by these tools are detailed in the following sections.

4.3 Coupled transport-burnup calculations using SCALE

4.3.1 SCALE Code System

The main tool will be used in this project, as mentioned previously, is the SCALE Code System [30] in its version 6.2.2, that was released in 2016. SCALE is a widely-used modeling and simulation suite for nuclear safety analysis and design that is developed and managed by Oak Ridge National Laboratory (ORNL).

SCALE provides a comprehensive, verified and validated tool set for criticality, reactor physics, radiation shielding and sensitivity and uncertainty analysis. This tool has been used since 1980 by regulators, licensees and research institutions around the world for safety analysis and design. SCALE include current nuclear data libraries and problem-dependent processing tools for continuous energy and multigroup neutronic calculations, as well as activation, depletion and decay calculations.

SCALE provides an integrated framework with many computational modules within different analysis areas. Two codes are presented as most interesting for trasnport-burnup

calculations, KENO-VI as the 3-D Monte Carlo transport code and ORIGEN as main activation, depletion and decay code.

In this sense, SCALE supports a wide range of reactor physics analysis capabilities coupling neutron transport calculations with ORIGEN to simulate the time-dependent transmutation of various materials. TRITON is the SCALE's modular reactor physics sequence for a wide variety of system types and it will be the used module to transport-burnup calculations.

4.3.2 TRITON

TRITON (Transport Rigor Implemented with Time-dependent Operation for Neutronic depletion) is a multipurpose SCALE control module for transport, depletion and sensitivity and uncertainty analysis for reactor physics applications. TRITON can be used to provide automated, problem-dependent cross sections processing followed by multigroup neutron transport for 1D, 2D and 3D configurations [30]. In addition, this functionality can be used in tandem with the ORIGEN depletion module and it will be the objective.

TRITON provides easy-to-use input options to define the time-dependent reactor condition as power history, material temperatures and materials compositions. Typically, TRITON has been used to perform deterministic transport analysis for 1D geometries and for 2D geometries using NEWT [22], the SCALE widely-known deterministic code.

In the latest release, TRITON has experimented notable improvements such as the capability to perform continuous energy transport calculations using Monte Carlo transport code KENO-VI. Multigroup treatment for this calculations existed in previous versions.

Several sequences are included in TRITON, each with its own design and applications; cross section processing, transport, depletion and sensitivity and uncertainty analysis. Depletion sequences included in TRITON (Table 4.5) are based on transport sequences with an automatic depletion/decay calculation after each transport calculation. TRITON automates the cross section processing, transport and depletion processes over a series of depletion and decay intervals supplied by the user.

The most interesting sequence within TRITON is called by '=T6-DEPL' sequence keyword. If multigroup treatment is required, XSProc will be the responsible module on preparing a problem-dependent MG cross section library. KENO-VI is used to 3D Monte Carlo transport calculations and ORIGEN is included as the inventory code.

One or more materials in the model can be designated for depletion and each selected material is depleted using region-averaged reaction rates, accounting for all regions in the model associated with a given depletion material. TRITON invokes the ORIGEN depletion module for the time-dependent transmutation of each defined material.

TRITON sequences for 3-D Monte Carlo burnup calculations present the computational flow shown in Figure 4.3. After each Monte Carlo transport calculation and

Sequence keyword	Main SCALE modules	Sequence function
=T-DEPL-1D	XSProc, XSDRNPM, ORIGEN, OPUS	1D MG deterministic transport, coupled with ORIGEN depletion
=T-DEPL	XSProc, NEWT, ORIGEN, OPUS	2D MG deterministic transport, coupled with ORIGEN depletion
=T5-DEPL	XSProc, KENO-V.a, ORIGEN, OPUS	3D Monte Carlo transport (KENO-V.a), coupled with ORIGEN depletion
=T6-DEPL	XSProc, KENO-VI, ORIGEN, OPUS	3D Monte Carlo transport (KENO-VI), coupled with ORIGEN depletion

Table 4.5: Depletion sequences available in TRITON [30].

post-processing by KMART module, TRITON provides ORIGEN the neutron flux space-energy distribution, multigroup cross sections if necessary, material concentrations and material volumes. ORIGEN performs the flux normalization, cross section collapse (COUPLE module) and multi-material depletion operations to determine new isotopic concentrations for the next step. This sequence is applied for each depletion time step imposed by the user. At the end, OPUS module is used to perform post processing and analysis on ORIGEN results.

TRITON sequence for 3-D Monte Carlo depletion calculations is based on the predictor-corrector approach. The depletion cycle is divided into various depletion intervals, in which the model power level is assumed constant. Within a depletion interval the isotope concentration of different depletion materials is modified, which induces changes in the neutron flux distribution, leading to different power distributions and transmutations rates in depletion materials. The user specifies easily the depletion scheme in TRITON.

The predictor-corrector approach performs cross section processing and transport calculations based on anticipated isotope concentrations at the middle-of-step of a depletion interval. Depletion calculations are then performed over the full interval using cross sections and flux distributions predicted at the middle-of-step. Burnup calculations are then extended to the middle-of-step of the next interval. The iterative process is repeated until all depletion intervals are processed.

Figure 4.4 illustrates in detail the predictor-corrector approach followed by TRITON. The algorithm can be structured on the following steps:

1. Cross section processing and a first transport calculation are performed at beginning-of-step t_0 using initial isotope concentrations.

2. Depletion *predictor* calculation from t_0 to the middle-of-step (MOS) of the first interval, determining isotope concentrations at MOS.

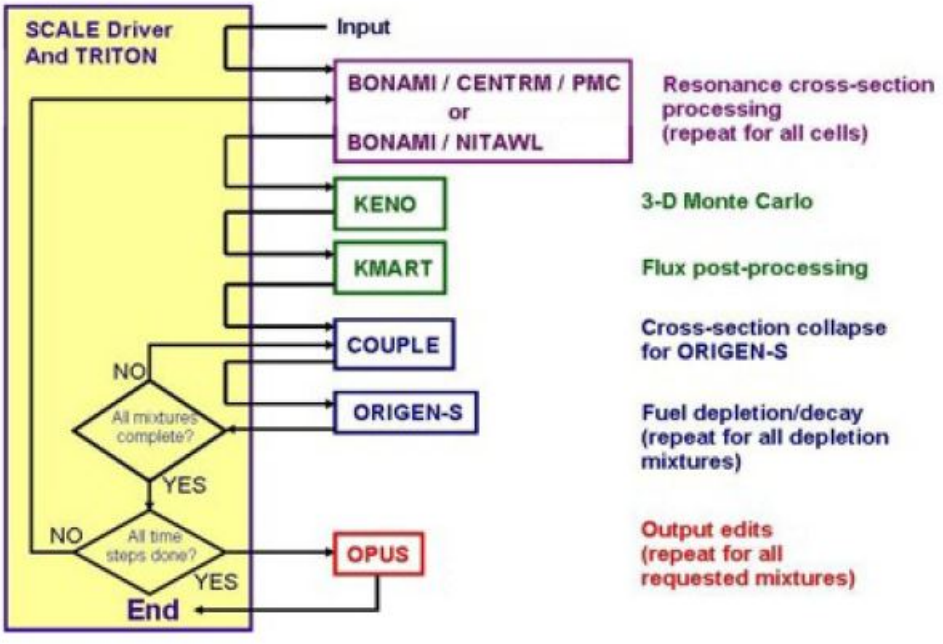

Figure 4.3: TRITON sequence for 3-D Monte Carlo burnup calculation [7].

3. Cross section processing and a new transport calculation are performed at MOS of the first interval.

4. Depletion *corrector* calculation for the first depletion interval is carried out in order to determine isotope concentrations at end-of-step (EOS) t_1.

5. A new depletion *predictor* calculation is performed at beginning-of-step of the second interval (t_1) is performed. This calculation use cross sections and flux distribution computed at the previous interval MOS.

6. The process continues in an iterative way repeating the previous steps. It is possible to include a decay interval, where power level is assumed zero, therefore transport calculation is not required.

Related to depletion equations resolution, ORIGEN includes two solvers kernels:

- MATREX, a hybrid matrix exponential/linear chains method.
- CRAM, a Chebyshev Rational Approximation Method

MATREX method is based in Equation 4.8 as Bateman equations notation. Exponential matrix is defined by the series expansion 4.9 with I as the identity matrix. For

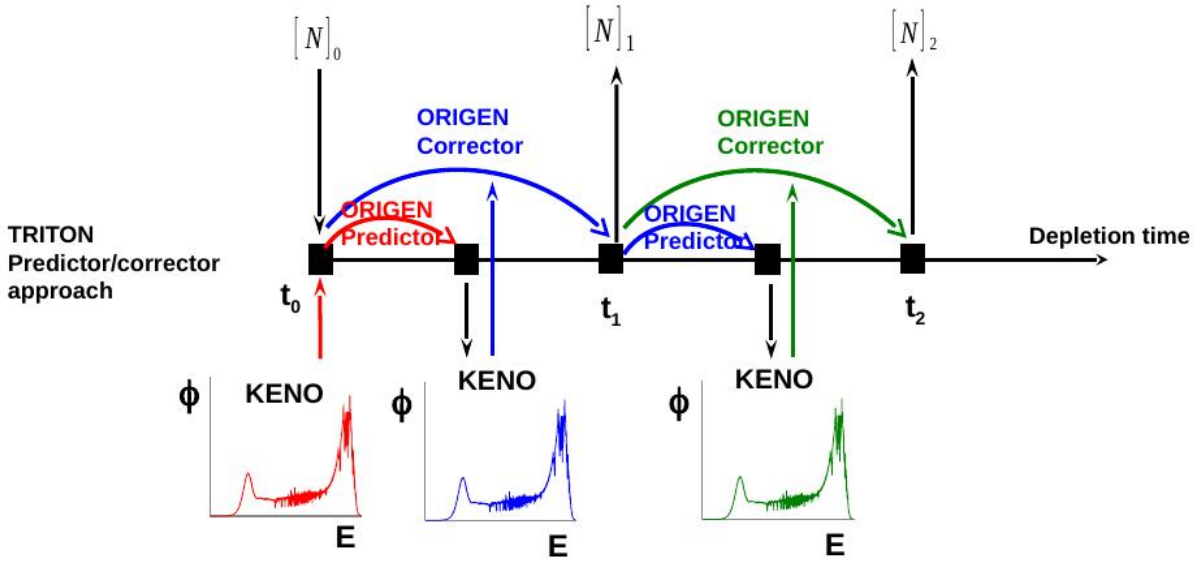

Figure 4.4: Predictor-corrector approximation followed by SCALE/TRITON.

computing the exponential matrix, the truncated Taylor series method is applied with scaling and squaring.

$$\dot{N}(\bar{r},t) = \exp(At) \cdot N(\bar{r},t) \tag{4.8}$$

$$\exp(At) = I + At + \frac{(At)^2}{2} + ... = \sum_{k=0}^{\infty} \frac{(At)^k}{k!} \tag{4.9}$$

By default, ORIGEN operates with MATREX method but the operation with CRAM method can be selected by the user. Both methods have similar runtimes but CRAM is more accurate and robust on a larger range of problems [30].

4.3.3 TRITON parameters

TRITON input is free-form and keyword based, similar in form to many other modules in SCALE. The input is organized into different blocks of data, which each one begins with *read blockname* and finishes with *end blockname*.

The first three lines of input contains the TRITON sequence name (=T6-DEPL) , the case title and the cross section library identifier. The library identifier *ce_v7.1_endf* is used for continuous energy calculations based on ENDF/B-VII.1 nuclear data library. If multigroup treatment is required, the identifiers *v7.1-252n* (252 groups) and *v7.1-56n* (56 groups) will be included in the input.

Parameter	Description
power	average specific power in the basis material(s), in MW per metric tonne of initial heavy metal (MW/MTHM)
burn	length of depletion interval in days
down	length of decay interval in days following the depletion interval
nlib	number of depletion subintervals for the depletion interval

Table 4.6: TRITON input: *BURNDATA* data block parameters description.

Material compositions are defined below and for multigroup calculations it is important to detail the parameters associated to resonance self-shielding. BONAMI and CENTRM/PMC are the modules for cross-section preparation within TRITON sequence. This step is not necessary for continuous energy calculations.

To introduce the depletion scheme, two data blocks are inevitably necessary: the *DEPLETION* and *BURNDATA* blocks. Firstly, the *DEPLETION* block specifies the materials for which depletion calculations are to be performed, in general fuel and target materials of interest. The user has to introduce the ID of materials will be depleted. By default, all TRITON depletion materials use the deplete-by-power mode but it may exist some situations where deplete-by-flux is more appropriate. In deplete-by-power mode, ORIGEN will determine the corresponding flux from the input-specific power, hence working in this mode a time-varying flux will result. The choice of approach is generally not an issue and significant differences are not expected between the two depletion modes.

The *BURNDATA* data block allows specification of the depletion scheme for the model. Parameters included within this data block are presented in Table 4.6. The depletion scheme consists of a series of depletion intervals or time intervals of constant power operation which may be partitioned into many depletion subintervals. Optionally, a decay interval -a time interval of zero-power- may be added to the scheme.

Obviously, power introduced within *BURNDATA* data block will be the power used by *DEPLETION* data block to determine the corresponding flux.

For depletion calculations, TRITON provides user control of the set of nuclides added to a fuel material through the *parm=(addnux=N)* control parameter. ORIGEN uses a 1-group cross section library and during depletion calculations, only cross sections for isotopes included in the transport calculation are updated on the 1-group library. For N=4, the selected and the most accurate option, a total of 388 nuclides are added to update cross sections in the ORIGEN depletion calculations. For this purpose, ORIGEN uses the flux provided by KENO to generate the 1-group cross section for all of 388 nuclides. Then, it is possible to track the impact of nuclides on cross section processing and depletion calculations.

Parameter	Description	Typical value
gen	nº of total generations	2.000
npg	nº of neutrons/histories per generation	50.000
nsk	nº of generations to be skipped	200
sig	k-eff standard deviation allowed	0.00015
tba	time allotted for each generation (in minutes)	60

Table 4.7: TRITON input: Monte Carlo parameters description.

Other data blocks can be added in the input: the *TIMETABLE* and the *OPUS* blocks. The *TIMETABLE* data block allows a detailed time-dependent description of some material properties (temperature and density) due to influences outside the depletion process. On the other hand, the *OPUS* data block is presented as useful tool to extract specific data from ORIGEN output libraries. The user can select the information to extract from ORIGEN output, allowing an easy visualization of time-dependent nuclide concentrations, mass or total thermal power associated.

Additionally, TRITON also requires the introduction of Monte Carlo parameters due to KENO-VI utilization. Monte Carlo parameters are included within *PARAMETER* data block and in Table 4.7 are presented the most relevant parameters.

KENO-VI performs three source convergence tests in order to check whether the problem has converged or not to a satisfactory k_{eff} value. These tests are repeated for all transport calculations carried out by TRITON depletion calculation. To consider acceptable the k_{eff} value obtained in each transport calculation, convergence tests have to be passed mandatorily.

4.3.4 Nuclear data libraries

KENO-VI neutron transport cross sections (in both CE and MG modes) are based on the ENDF/B-VII.1 nuclear data.

ORIGEN needs nuclear decay data, neutron reaction cross sections and neutron-induced fission product yields [30].

- The nuclear decay data are based on ENDF/B-VII.1 library including half-lives, decay modes and decay branching fractions (*origen.rev03.decay.data*).
- Related to neutron reaction cross sections, ORIGEN library (*origen.rev01.jeff252g*) is based on the JEFF-3.0/A nuclear data library. Cross section data from this library are converted to point-wise cross section data which are collapsed using the typical

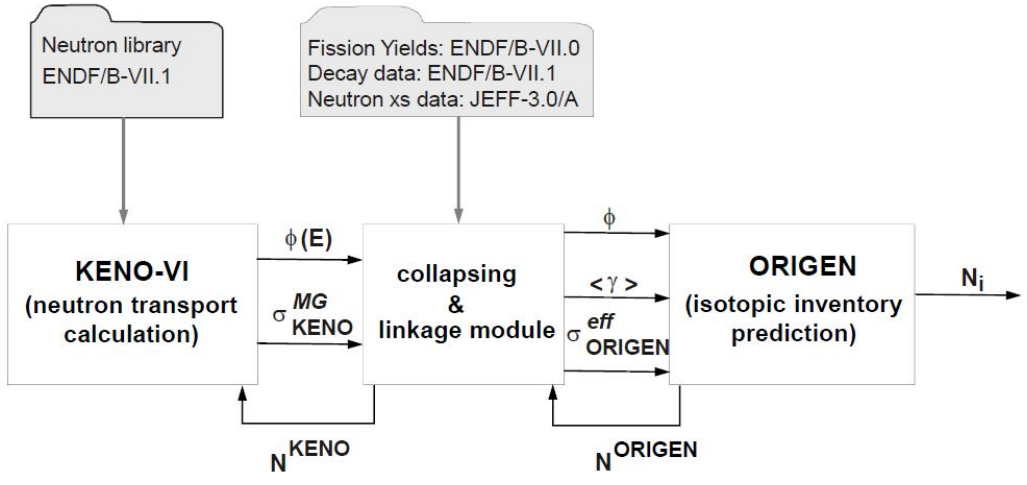

Figure 4.5: SCALE methodology for coupled transport/depletion calculations.

thermal spectrum to different group structures, 252-group by default. With respect to the JEFF-3.0/A, ORIGEN library includes a modification relative to the Am-241 branching ratio to the Am-242 ground and metastables states. The branching ratio of Am-241 to Am-242m is modified from 8.2% to 10.0% which is based on ENDF/B-VII.0.

- At last, the fission-yield resource contains the energy-dependent yields of each fission product for 30 fissionable actinides. Fission yields are obtained from the ENDF/B-VII.0 data library and they are available for thermal, fast and high-energy incident neutron energies (*origen.rev05.yields.data*).

Figure 4.5 shows clearly the full KENO/ORIGEN coupled sequence with the used nuclear data libraries in this work. For neutron transport calculation performed by KENO-VI the ENDF/B-VII.1 library is the used one. ORIGEN receives the flux spectrum and multigroup cross sections provided by KENO to generate the one-group cross sections. Then, ORIGEN performs the depletion calculations based on different libraries for fission yields, decay data and neutron cross-section data. As a result, new nuclide compositions calculated by ORIGEN are given to KENO if the depletion cycle is not finished.

4.4 Coupled transport-burnup calculations using Serpent

Though SCALE is the main tool employed in this project, Serpent [4] has been used as a reference code to support calculations performed by SCALE. Serpent is a widely-used

neutronic code, also by other partners within ESFR-SMART project. In this section, a brief introduction to Serpent code is presented and a detailed approximation to Serpent transport-burnup calculations will be carried out.

4.4.1 Serpent

Serpent [25] is a three-dimensional continuous-energy Monte Carlo reactor physics burnup calculation code. This code was developed and is maintained by VTT Technical Research Centre of Finland since 2004. Serpent started out as a simplified reactor physics code but the capabilities of current versions extend well beyond reactor modeling. The current version of the code is Serpent2 and, concretely, in this project Serpent 2.1.29 will be the used version.

Serpent main applications are related to traditional reactor physics: criticality calculations, fuel cycle studies or validation of deterministic transport codes. Moreover, Serpent presents other applications such as multi-physics simulations (i.e. coupled calculations with thermal hydraulics) or neutron and photon simulations for radiation dose rate calculations.

Similar to other Monte Carlo codes, the basic geometry description in Serpent relies on an universe-based constructive solid geometry, allowing the description of any two- or three-dimensional fuel or reactor configuration. Taking into account the ASTRID core design -hexagonal sub-assemblies and a large axial heterogeneity-, an easy geometry treatment is very valuable.

Particle transport in Serpent is based on the combination of conventional surface-tracking and the Woodcock delta-tracking method. The tracking routine has proven efficient and well suited for systems with fuel assemblies, including systems which works with micro-particle fuels.

As mentioned previously, Serpent is a code widely-used by research institutions. In fact, within ESFR-SMART project, Serpent will be used for initial core performance study, burnup calculations and also for safety and performance parameters calculation at end-of-cycle.

4.4.2 Transport-burnup calculations

Serpent follows a predictor-corrector method for coupled transport-burnup calculations. This method shares the name with the method followed by ORIGEN but is not similar in operation.

Figure 4.6 shows the predictor-corrector approximation followed by Serpent. The algorithm is divided into the following steps:

1. As TRITON algorithm, in this case a first transport calculation is also performed at beginning-of-step (BOS). Neutron flux at BOS ϕ_0 is determined.

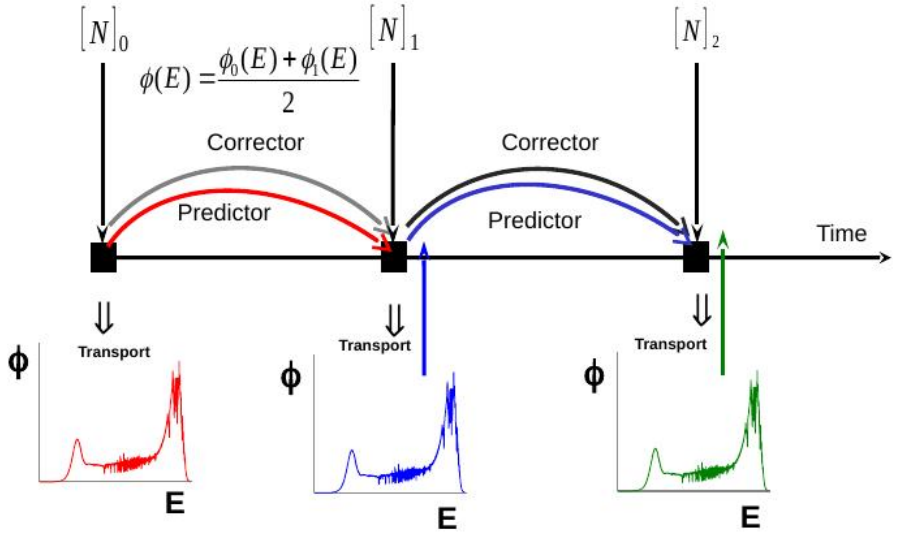

Figure 4.6: Predictor-corrector approximation followed by Serpent.

2. A depletion *predictor* calculation is carried out in order to determine the isotopic composition at end-of-step (EOS).

3. With the new isotopic composition, a new transport calculation is performed. Neutron flux ϕ_1 at EOS is calculated.

4. A depletion *corrector* calculation is performed with the average flux between the BOS and EOS, $\bar{\phi}(E) = \frac{1}{2}(\phi_0(E) + \phi_1(E))$. Then, isotopic composition is determined at EOS.

5. The process continues in an iterative way for different depletion steps established.

It is important to note a basic difference between predictor-corrector approaches followed by Serpent and TRITON. If the user establishes the same depletion scheme for Serpent and TRITON calculations, criticality values for different time steps will be obtained. Serpent will provide k_{eff} value for real time steps while TRITON will provide this parameter at middle of step. However, k_{eff} value will be provided by both codes at the beginning of full depletion cycle t_0.

Related to resolution of depletion equations, Serpent has three options and two methods for solving the Bateman equations. The first method is Transmutation Trajectory Analysis (TTA), based on the analytical solution of linearized transmutation chains. The second method is an advanced matrix exponential solution based on the CRAM method mentioned previously. The third option is related to first method, changing the way on solving TTA equations.

As explained in the previous section, the method for solving the Bateman equations followed by ORIGEN is based on the truncated Taylor series for the matrix exponential resolution. In this case, CRAM will be the used method and it is based on the observation that the eigenvalues of the depletion coefficient matrix A are confined around the negative real axis [28].

Several comparisons between different methods have been carried out and it is proven that CRAM method presents advantages in terms of accuracy and running time with respect to TTA methods [24]. Compared to ORIGEN solver, CRAM presents an higher accuracy but also higher running time, that may be a limiting factor. In order to compare results provided by both solvers, a detailed isotopic compositions comparison will be presented in the following chapters.

4.4.3 Serpent parameters

Basically, the additional input for burnup calculations consists of identifying the depleted materials and setting up the irradiation history. Material composition, geometry definition and Monte Carlo parameters are similar to inputs for basic criticality calculations. Moreover, some additional parameters for determining file paths and options used by the calculations routines are available.

Serpent input is divided into a series of cards; *cell*, *lat*, *pin* and *surf* cards for geometry definition, *mat* card for material compositions and the *dep* card for irradiation history definition. The *set* command is dedicated to fix different parameters and file paths where cross section library or decay and fission yield libraries are located.

Firstly, the irradiation history or the burnup cycle has to be detailed by the *dep* card and different options allow data introduction. The most intuitive option is *daytot*, which allows the depletion step definition in cumulative time. Previously, it is required to define the total power (*power*) or the power density (*powdens*).

Table 4.8 shows the main parameters that the user has to define in the input. Related to resolution of depletion equations, the user can select the solution method by the *bumode* option: (<mode>=1) for TTA method, (<mode>=2) for CRAM method and (<mode>=3) for TTA modified method. CRAM method will be the option selected. Moreover, the predictor-corrector method is called by the *pcc* option and fixing <flag>=1.

For calculating the isotopic one-group transmutation cross sections, the user can fixed the employed method by the *xscalc* option. By default, the codes calculates these parameters using a high-resolution flux spectrum recorded during the transport calculation (<mode>=2).

At last, the *inventory* option allows a personalized output generation. This option is followed by a list of numerical values that identify the nuclides will be included in the output. Additionally, using the *printm* option with <mode>=1, independent outputs with the compositions of depleted materials will be generated.

Option	Description	Input format
declib	file path for radioactive decay data	*set declib* "file path"
nfylib	file path for fission yield data	*set nfylib* "file path"
bumode	solution method for Bateman equations	*set bumode* <mode>
pcc	flag for predictor-corrector calculation	*set pcc* <flag>
xscalc	transmutation cross sections generation	*set xscalc* <mode>
printm	flag for printing material compositions	*set printm* <mode>
fpcut	fission product yield cut-off	*set fpcut* <lim>
stabcut	stability cut-off	*set stabcut* <lim>
inventory	nuclide list for burnup calculation output	*set inventory* <id1>...

Table 4.8: Serpent input: List of relevant parameters and options in burnup calculations.

Finally, Monte Carlo calculations are controlled by the following card:

set pop <npop> <cycles> <skip>

With <npop> as the number of source neutrons per cycle, <cycles> as the number of active cycles run and <skip> as the number of inactive cycles run.

4.4.4 Nuclear data libraries

Since Serpent is used for benchmarking of SCALE results, neutron transport libraries are based on ENDF/B-VII.1 nuclear data.

Concerning depletion calculations, Serpent requires moreover nuclear decay data and neutron-induced fission product yields:

- The nuclear decay file is ENDF/B-VII.1 library.
- The fission-yield data library contains the energy-dependent yields of each fission product for 31 fissionable nuclides. These fission yields are based on the ENDF/B-VII.1 data library and they are structured into three groups.
- If energy-dependent branching ratios are to be used, the branching data library based on the JEFF-3.1/A can be used (FILE 3).

SCALE		Serpent
ENDF/B-VII.1	Neutron library	ENDF/B-VII.1
ENDF/B-VII.0 (*)	Fission yields library	ENDF/B-VII.1
ENDF/B-VII.1	Decay data library	ENDF/B-VII.1
JEFF-3.0/A (**)	Branching ratios library (special purpose)	JEFF-3.1/A

Table 4.9: Nuclear data libraries used by SCALE and Serpent for each purpose.

As a summary, Table 4.9 collects the main information related to nuclear data libraries used by each code.

(*) Some modifications were adopted to address inconsistencies between the direct and cumulative fission yields for U-235, U-238 and Pu-241 and neutron energy had been adjusted from 500 keV to 2 MeV.

(**) Several minor modifications were adopted using the ENDF/B-VII.0 data: 1) Np-239 radiative neutron capture cross section and 2) Am-241 branching ratios to Am-242g/m.

Chapter 5

Simplified 3D pin-cell Monte Carlo burnup calculations

5.1 Introduction

Firstly, calculations will be carried out for a simplified model with the aim of predicting the trends of different results for full core calculations. Moreover, this case will be useful in order to visualize the multigroup effect over SCALE/TRITON calculations. A detailed comparison between MG and CE calculations performed by SCALE/TRITON will provide an initial idea about the adaptation of MG libraries (56 and 252 groups) for fast neutron spectrum calculations.

On the other hand, by comparing the inventory results along the depletion cycle, consideration of radiative capture reaction ratios and fission yields by each code can be assessed. The treatment followed by SCALE/TRITON and by Serpent is studied in order to establish the more realistic application of the branching ratios.

5.2 Simplified pin-cell of the inner zone

Figure 5.1 depicts the radial layout of the pin-cell included in the inner zone of the ASTRID core. The employed model is a simplified 3D pin-cell with an axial length very much larger than radial dimensions. It is very useful in terms of calculation times with respect to 2D model due to adopted boundary conditions; reflective in the radial direction and void in the axial direction. Therefore, some neutron leakages will take place in the axial direction, reducing considerably the calculation time.

Axial heterogeneity detail is neglected, reducing the pin-cell just to the fissile zone. The MOX-IZ which has been defined at beginning-of-life in Table 3.1 is included as fuel material. Radial dimensions of the pin-cell, evaluated at normal operating conditions, are presented in Table 5.1.

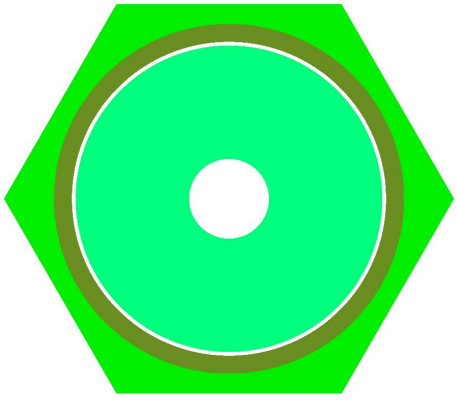

Figure 5.1: Radial layout of the 3-D pin-cell model.

Parameter	Value
Fuel inner hole diameter	0.223 cm
Fuel pellet diameter	0.856 cm
Inner cladding diameter	0.877 cm
Outer cladding material	0.977 cm
Pin pitch	1.088 cm

Table 5.1: Pin-cell characteristics at nominal operating conditions.

In this case, temperatures for cross sections calculations are 1200K for fuel material and 600K for the rest ones, cladding material and sodium coolant. These temperatures are not the real temperatures at normal operating conditions but cross sections libraries are available at these temperatures. By selecting these values, the interpolation that SCALE/TRITON would perform between selected value (1500K at normal operating conditions) and available value (1200K in this case) is avoided.

5.3 Depletion scheme and expected results

The adopted depletion scheme is based on other benchmarks such as [14] where a comparison between several codes (Serpent, MCNP and ECCO/ERANOS) and different nuclear data libraries has been carried out for the SFR fresh sub-assembly.

The depletion cycle consists of 410 days with a constant thermal power density of

50.4 MW/tHM. The cycle is divided into 4 sub-intervals of 102.5 days each one, hence five Monte Carlo transport calculations will be performed by both codes. Additionally, a decay step of 60 days is added in order to assess the branching ratios for decay and not only for capture.

Related to expected results, several parameters may be compared but the results will be analyzed along the depletion cycle are:

- Multiplication factor k_{eff},
- Neutron flux level,
- Nuclides densities of interesting materials at the cumulative burnup steps,
- Branching ratios for capture reactions, e.g. (Am-241→Am-242g/m) and branching ratios for decay, e.g. (Am-242→Pu-242),
- Calculation time for each case.

As explained in Chapter 4, using TRITON sequence, it is not possible to get both nuclide composition and multiplication factor at the same depletion step. Consequently, k_{eff} values performed by TRITON will not correspond in time to the ones performed by Serpent. To achieve the same time evolution, the depletion cycle is completed until 410 days by linear interpolation for TRITON results.

Nuclide composition can be compared at the same depletion steps without restrictions and any interpolation is not necessary. Only the most interesting nuclides are presented for each case and a detailed comparison between TRITON-CE and Serpent calculations is included in Section 5.6.

5.4 SCALE/TRITON calculations

5.4.1 MG calculations

In order to assess the adaptation of SCALE MG libraries to fast neutron spectrum calculations, simulations are performed using the two MG structures included in SCALE 6.2.

Based on ENDF/B-VII.1 nuclear data library, SCALE includes a fine group structure for criticality safety and reactor physics applications, the 252-group library. This structure was developed to adequately capture spectral and temperature effects important for reactor systems and was processed with newer procedures [30]. With respect to the widely-used 238-group structure, the 252-group library presents several enhancements in the MG processing procedures. While the 238-group library is processed using the standard weighting function (Maxwellian + $1/E$ + Watt Fission spectrum at 1.273 MeV + $1/E$), the 252-group library presents the following improvements:

- For actinide materials (Z>89), the base weighting function is computed by the pointwise transport code CENTRM for a PWR spectrum. The standard function is still used for materials with Z<90. Then, the 252-group library provides a more detailed representation of the U-238 resonances structure.
- The thermal energy range which includes up-scattering reactions is extended to $5\,eV$, compared to $3\,eV$ in the 238-group library.

Related to the energy structure, 238-group and 252-group libraries are practically similar throughout the fast neutron spectrum (from $10^4\,eV$ to $10^7\,eV$ approximately).

On the other hand, the 56-group structure is available mainly for LWR physics calculations with a fine group structure around the thermal zone of the energy spectrum. Though this structure is optimized for LWR, calculations for fast spectrum are performed with the objective of identifying possible differences with respect to CE calculations. A SFR-optimized MG library may be necessary taking into account the significant calculation time reduction compared to CE calculations.

Based on the depletion scheme that has been described in Section 5.3 and using as Monte Carlo parameters which are presented in Table 4.7, calculations with both MG libraries are performed. Deplete-by-power mode is selected for the fuel material, hence a time-varying neutron flux is obtained.

Table 5.2 collects the multiplication factor evolution performed by TRITON with 56-group and 252-group libraries. Multiplication factor statistical error is about 10 pcm for all TRITON calculation, both in MG and CE mode.

At first sight not very large differences between both MG libraries are observed. At the initial burnup step, a difference of 107 pcm is obtained and both calculations present a similar evolution along the depletion cycle. Related to nuclide concentrations performed by ORIGEN in each depletion time step, no relevant variations between both libraries are observed.

Therefore, using the simplified model, both MG libraries present a similar behaviour. The adaptation of MG libraries for fast spectrum calculations can be assessed by comparing with CE calculations performed below.

5.4.2 CE calculations

The continuous energy treatment in SCALE provides high resolution solution strategies by representing the resolved resonance region by pointwise data where the energy point density is optimized for each reaction of each nuclide [30]. Data in the unresolved resonance region are represented by probability tables, and data above this region implement pointwise data with explicit point-to-point representation. Moreover, resonance upscattering techniques are implemented via the Doppler Broadened Rejection Correction (DBRC) method that was assessed by [10]. By applying this method, a reactivity

Burn-up step [days]	0	51.25	153.75	256.25	358.75	410
56-group k_{eff} [-]	1.38268	1.37597	1.36429	1.35276	1.34146	1.33557
252-group k_{eff} [-]	1.38161	1.37521	1.36412	1.35296	1.34186	1.33619
CE k_{eff} [-]	1.37885	1.37276	1.36156	1.35042	1.33945	1.33382

Table 5.2: Results for pin-cell burnup calculations with SCALE/TRITON (Standard deviation of computed values: ±10 pcm for MG and ±14 pcm for CE).

Burn-up step [days]	0	51.25	153.75	256.25	358.75	410
Δk_{eff} [pcm]	276	245	256	254	241	236

Table 5.3: Multiplication factor difference between TRITON-252g and TRITON-CE calculations.

correction of approximately 300 pcm was determined relative to the default methodology for a LWR fuel pin with elevated temperatures (1200 K).

DBRC method has been applied to the MOX fuel pin-cell model (1200 K) and no relevant differences (less than 10 pcm) are encountered relative to the default methodology. This conclusion is confirmed for full core calculations too. Thus, the default methodology is the applied one throughout this project.

Therefore, a TRITON-CE calculation is conducted using the ENDF/B-VII.1 cross section library with the same parameters than TRITON-MG input. Table 5.2 provides the evolution of multiplication factor along the depletion scheme obtained by this calculation.

5.4.3 MG effect assessment

A detailed comparison between MG libraries included in SCALE 6.2 and CE treatment was carried out by [11], concluding that the 252-group library does not work well for MOX fuel in a SFR sub-assembly. Therefore, in this subsection, the objective is to demonstrate that conclusion and to explain the limitations of the 252-group library for fast spectrum calculations.

Firstly, Figure 5.2 shows the multiplication factor evolution along the depletion scheme obtained by the three different cases. As it can be observed, the 252-group calculations show differences of about 230-280 pcm (see Table 5.3) with the CE ones along the cycle.

This disagreement can also be observed when comparing the neutron flux along the depletion cycle (see Figure 5.3). As it can be expected, the neutron flux increases in each depletion time step due to the selected depletion-by-power mode.

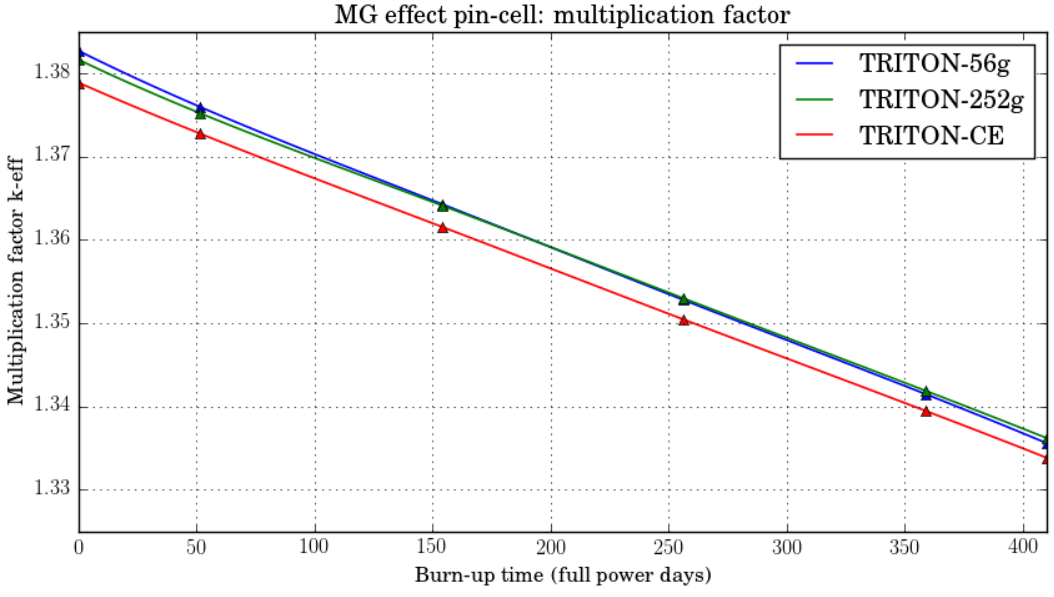

Figure 5.2: Comparison of k_{eff} evolution obtained by TRITON-MG libraries and by TRITON-CE for the pin-cell model.

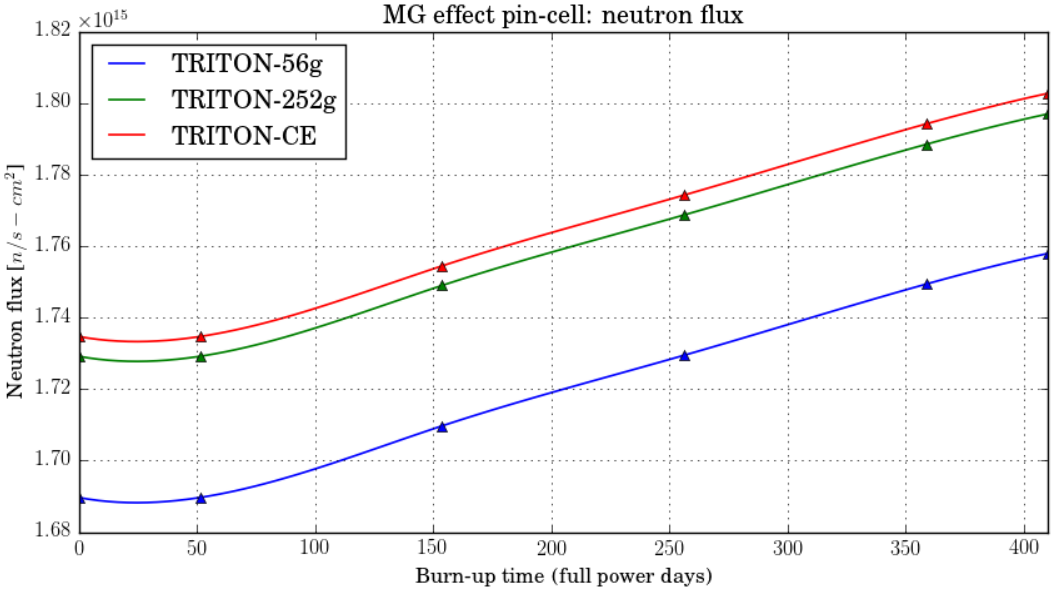

Figure 5.3: Comparison of neutron flux evolution obtained by TRITON-MG libraries and by TRITON-CE for the pin-cell model.

Burn-up step [days]	0	102.5	205	307.5	410	470
U-234	0.00%	-0.01%	-0.01%	-0.01%	-0.02%	-0.01%
U-235	0.00%	-0.00%	-0.00%	-0.01%	-0.01%	-0.01%
U-238	0.00%	0.00%	0.00%	0.01%	-0.01%	0.01%
Np-237	0.00%	-0.18%	-0.39%	-0.35%	-0.28%	-0.27%
Pu-238	0.00%	0.00%	-0.01%	-0.01%	-0.02%	-0.02%
Pu-239	0.00%	0.00%	-0.01%	-0.01%	-0.02%	-0.02%
Pu-241	0.00%	-0.01%	-0.01%	-0.02%	-0.03%	-0.03%
Am-241	0.00%	0.00%	0.00%	0.01%	0.01%	0.01%
Am-242	0.00%	-0.15%	-0.13%	-0.16%	-0.13%	-0.18%
Am-242m	0.00%	-0.19%	-0.18%	-0.18%	-0.18%	-0.18%
Am-243	0.00%	0.12%	0.12%	0.12%	0.12%	0.12%
Cm-245	0.00%	-0.28%	-0.25%	-0.28%	-0.27%	-0.27%
Cm-246	0.00%	-0.50%	-0.46%	-0.49%	-0.48%	-0.49%

Table 5.4: Relative deviation of nuclides densities obtained by TRITON-252g and by TRITON-CE.

In order to compare the nuclide densities of fuel at the cumulative burnup steps, a relative deviation (Equation 5.1) between the two cases of interest is defined.

$$Relative\,deviation\,(\%) = \frac{TRITON/252g - TRITON/CE}{TRITON/CE} \cdot 100 \tag{5.1}$$

In this sense, a good agreement between TRITON-252g and TRITON-CE nuclide densities along the depletion cycle is obtained (see Table 5.4). It would be expected because calculations are performed by the same code and the same nuclear data library. Therefore, small bandwidths obtained for nuclide densities are only caused by MG structure. More relevant results may be extracted by comparing different codes, where different branching ratios treatment may have an important effect.

An analysis of the neutron flux in the MOX fuel region of the pin-cell is performed in order to determine why the 252-group library does not work adequately for fast application. For this purpose, the *flx* KENO-VI parameter was set to "yes" in the TRITON input. Then, neutron flux and fission/absorption distributions are collected in the *.kmt* data files (*kmart_flux0001.kmt* and *kmart_fisabs0001.kmt*) into the .htmd directory for each depletion time step. These data files are generated by the KMART (Keno Module for

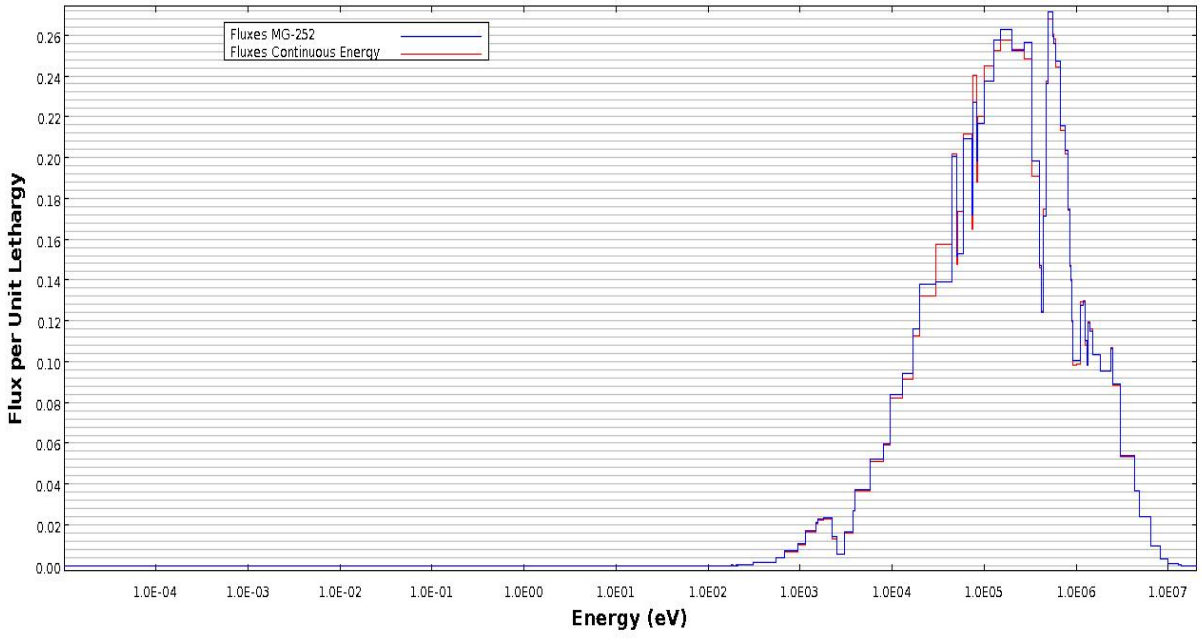

Figure 5.4: Neutron flux spectrums obtained by TRITON-252g and by TRITON-CE for the MOX material in the pin-cell.

Activity-Reaction Rate Tabulation) module incorporated within the TRITON sequence.

The *.kmt* data files can be handled easily by the *Javapeño* data visualization tool and Figures 5.4 and 5.5 were generated using this tool. These distributions correspond to the beginning of the depletion cycle, that it is the first Monte Carlo calculation. Note that the CE neutron flux distribution is collapsed to the same 252-group structure defined in the MG library.

As shows Figure 5.4, the flux decreases in the vicinity of the Na elastic scattering resonance (around 3 keV) and increases at low energies because of U-238 and Pu-239 resonances. The 252-group flux distribution follows adequately the CE solution for low ($< 10^4\, eV$) and high ($> 10^6\, eV$) energies. At the center region of the spectrum a clear disagreement between both flux distributions can be observed. This disagreement leads to the multiplication factor difference which has been obtained previously.

Moreover, Figure 5.5 confirms via fissions and absorptions production the spectrum zone where the 252-group library diverges with the CE solution. Therefore, it is clear that the MG library does not work with enough accuracy for fast neutron spectrum.

For a meaningful comparison, both the KENO-CE and KENO-MG results can be collapsed to one group. Moreover, for the reaction cross-section of interest, also KENO-CE results can be collapsed to match the MG structure of the KENO-MG output.

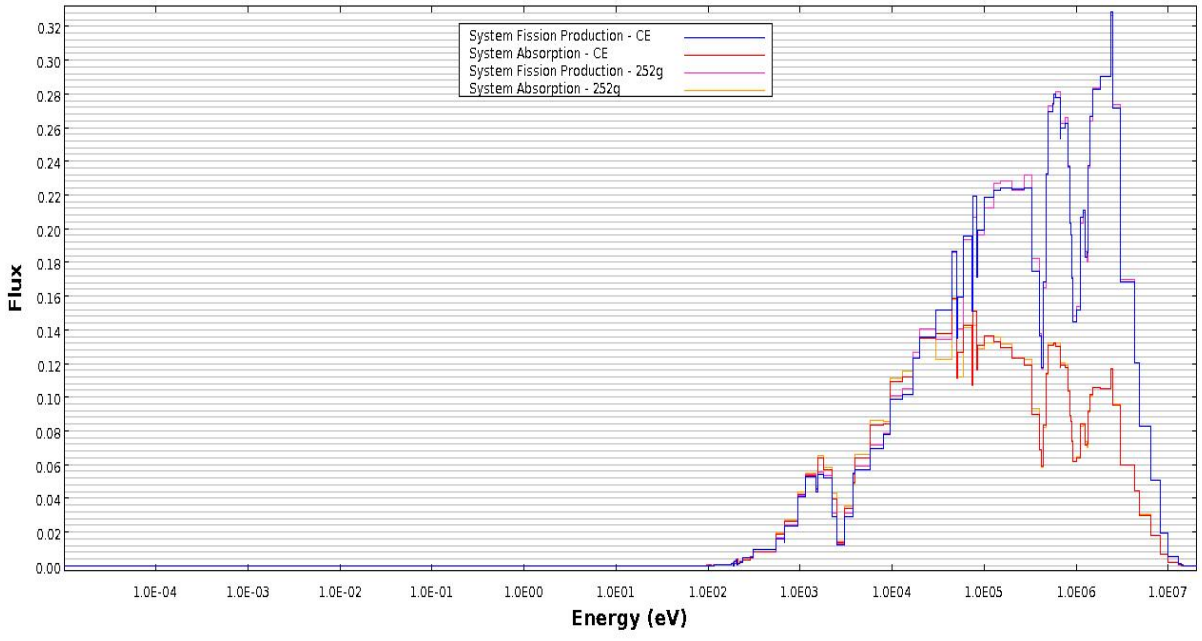

Figure 5.5: Fission and absorption spectrums obtained by TRITON-252g and by TRITON-CE for the MOX material in the pin-cell.

In order to identify the main reactions that have an important influence over the disagreement between KENO-CE and KENO-MG calculations, the problem-dependent reaction rates are collapsed to one-group.

Related to KENO-CE, it is possible to compute different tallies: reaction rates, flux and reaction cross sections. The block *READ REACTION* is used for this task, where besides the type of tally, the reaction/nuclide pairs for tally calculations has to be specified. This block can be used together with:

- The *READ ENERGY* block, where the energy group boundaries are specified. It sets NGP value. If only one energy group is given, this is equivalent to option *cxm=1* (obsolete in SCALE 6.2, but with the same meaning, that is, tally cross sections and reactions rates in NGP=1 group).

- If only NGP is specified (without the *READ ENERGY* block), and NGP is equal to the number of energy groups in one SCALE cross section library, that energy group structure will be used for tallying. Different group structures are available in SCALE, one of them in 200-groups, adequate for fast applications. However in this work, the 252-group structure was used to match the MG structure of the KENO-MG output.

Concerning the KENO-MG results, KMART6 post-processing tool has to be used. It allows collapsing fluxes and reaction rates calculated by KENO.

Therefore, Table 5.5 collects the reaction rates for the most important reactions of fuel, coolant and cladding main nuclides. By using the CE results as reference, it is interesting to assess the possible deviations that MG results present.

In this sense, Figure 5.6 depicts the deviations of a selection of these reaction rates between KENO-CE (as reference) and KENO-MG. As it can be observed, capture reaction rate of Pu-239 and inelastic reactions present a relevant difference. Moreover, as obtained by [13], there are remarkable bandwidths for elastic scattering of Na-23 (coolant) and Fe-56 (included within the ODS cladding material). It can be concluded that KENO-MG overestimates the main reaction rates with respect to KENO-CE.

Nevertheless, as it can be seen in Figure 5.7, there is a common trend related to the elastic scattering reactions of the U, Pu and Am isotopes. KENO-MG reports a lower value than the performed one by KENO-CE for this type of reaction.

Reactions which present the clearest deviations can be analysed in depth via group and energy-dependent cross sections or reactions rates. For this purpose, the 252-group collapsed reactions rates for neutron capture of Pu-239, inelastic scattering of U-238 and elastic scattering of Fe-56 and Na-23 are presented in Figure 5.8. As it can be observed for all these reactions, the 252-group library is not capable to preserve the detail that KENO-CE results show.

Concerning the Pu-239 neutron capture, it can be noted that the more important deviations ($10\,keV$ to $400\,keV$) correspond to the unresolved resonance range of this reaction cross section.

Deviations for inelastic scattering of U-238 are mainly presented in the energy region from $100\,keV$ to $1\,MeV$. KENO-MG is not capable to reproduce very well the KENO-CE results below the $^{238}U(n,n')$ threshold.

On the other hand, deviations for Na-23 and Fe-56 elastic scattering reactions correspond to the resonance energy region ($10\,keV$ to $400\,keV$). In both cases, these differences are located in the resolved range of cross section data.

Moreover, SCALE allows to compute the expected change in k_{eff} due to a change in the cross section of each reaction and each nuclide. As analysed by [5] via integrated sensitivity coefficients[1] (ISC), reactions such as $^{239}Pu(n,\gamma)$, $^{238}U(n,n')$ and $^{23}Na(n,n)$ have an important role over the k_{eff} value. Therefore, it can be concluded that differences between KENO-MG and KENO-CE k_{eff} values are caused by the deviations of these reaction rates.

[1]The integrated sensitivity coefficients of k_{eff} ($\frac{\Delta k/k}{\Delta\Sigma/\Sigma}$) are computed using the TSUNAMI control module implemented within SCALE.

Nuclide	Reaction	252-g collapsed to 1G react. rate $[n/cm^3s]$	CE collapsed to 1G react. rate $[n/cm^3s]$	Relative deviation [%]
U-235	elastic	$3.0479 \cdot 10^{-4}$	$3.0615 \cdot 10^{-4}$	-0.44
	inelastic	$3.2087 \cdot 10^{-5}$	$3.1838 \cdot 10^{-5}$	0.78
	fission	$6.5752 \cdot 10^{-5}$	$6.5687 \cdot 10^{-5}$	0.10
	(n,γ)	$1.7564 \cdot 10^{-5}$	$1.7527 \cdot 10^{-5}$	0.21
U-238	elastic	$1.7577 \cdot 10^{-1}$	$1.7649 \cdot 10^{-1}$	-0.41
	inelastic	$2.0483 \cdot 10^{-2}$	$2.0328 \cdot 10^{-2}$	0.76
	fission	$1.0063 \cdot 10^{-3}$	$1.0046 \cdot 10^{-3}$	0.17
	(n,γ)	$4.5449 \cdot 10^{-3}$	$4.5426 \cdot 10^{-3}$	0.05
Pu-239	elastic	$2.7282 \cdot 10^{-2}$	$2.7392 \cdot 10^{-2}$	-0.40
	inelastic	$2.9908 \cdot 10^{-3}$	$2.9838 \cdot 10^{-3}$	0.23
	fission	$5.6749 \cdot 10^{-3}$	$5.6671 \cdot 10^{-3}$	0.14
	(n,γ)	$1.2773 \cdot 10^{-3}$	$1.2670 \cdot 10^{-3}$	0.81
Pu-240	elastic	$1.4181 \cdot 10^{-2}$	$1.4239 \cdot 10^{-2}$	-0.41
	inelastic	$1.3942 \cdot 10^{-3}$	$1.3858 \cdot 10^{-3}$	0.60
	fission	$6.3820 \cdot 10^{-4}$	$6.3589 \cdot 10^{-4}$	0.36
	(n,γ)	$6.4543 \cdot 10^{-4}$	$6.4587 \cdot 10^{-4}$	-0.07
Pu-241	elastic	$3.1788 \cdot 10^{-3}$	$3.1939 \cdot 10^{-3}$	-0.47
	inelastic	$4.2760 \cdot 10^{-4}$	$4.2416 \cdot 10^{-4}$	0.81
	fission	$1.0096 \cdot 10^{-3}$	$1.0077 \cdot 10^{-3}$	0.18
	(n,γ)	$1.5423 \cdot 10^{-4}$	$1.5387 \cdot 10^{-4}$	0.23
Pu-242	elastic	$4.7779 \cdot 10^{-3}$	$4.7980 \cdot 10^{-3}$	-0.42
	inelastic	$4.3564 \cdot 10^{-4}$	$4.3302 \cdot 10^{-4}$	0.61
	fission	$1.4331 \cdot 10^{-4}$	$1.4259 \cdot 10^{-4}$	0.51
	(n,γ)	$1.6516 \cdot 10^{-4}$	$1.6469 \cdot 10^{-4}$	0.29
Am-241	elastic	$6.2412 \cdot 10^{-4}$	$6.2656 \cdot 10^{-4}$	-0.39
	inelastic	$5.8898 \cdot 10^{-5}$	$5.8448 \cdot 10^{-5}$	0.77
	fission	$2.2796 \cdot 10^{-5}$	$2.2718 \cdot 10^{-5}$	0.34
	(n,γ)	$1.1597 \cdot 10^{-4}$	$1.1593 \cdot 10^{-4}$	0.03
Na-23	elastic	$1.0742 \cdot 10^{-1}$	$1.0690 \cdot 10^{-1}$	0.49
Fe-26	elastic	$2.2036 \cdot 10^{-1}$	$2.1918 \cdot 10^{-1}$	0.54

Table 5.5: Collapsed one-group reaction rates of the 3D pin-cell model.

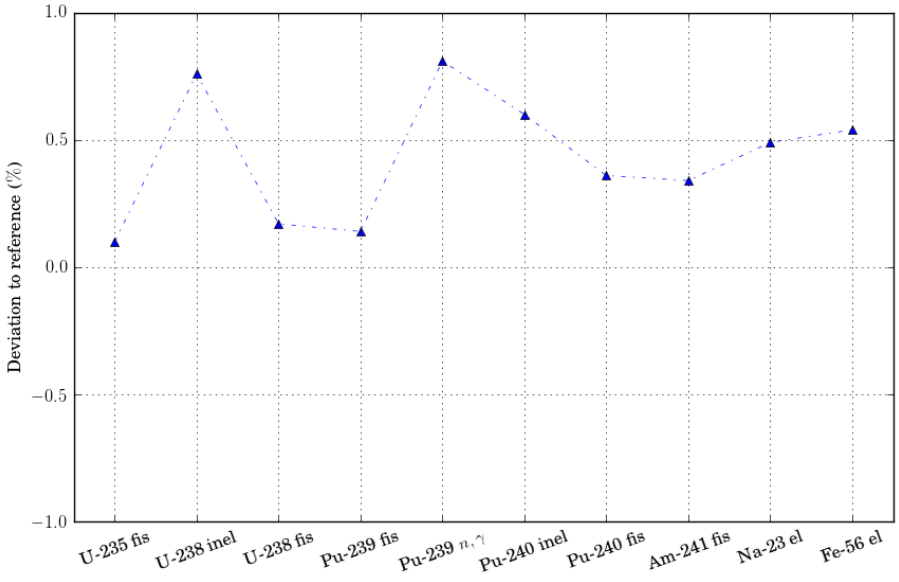

Figure 5.6: Collapsed one-group reaction rates of the 3D pin-cell compared to the CE reference.

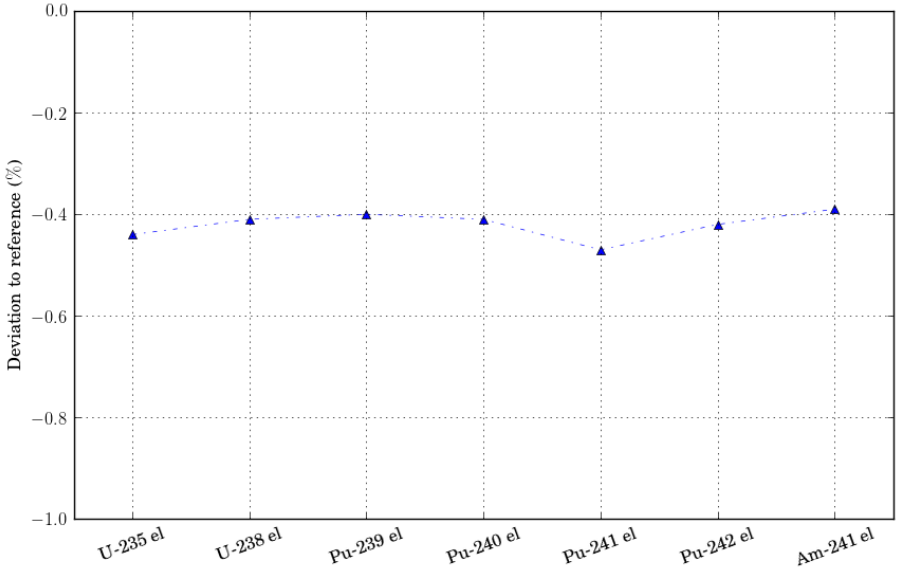

Figure 5.7: Collapsed one-group elastic reaction rates of the 3D pin-cell compared to the CE reference.

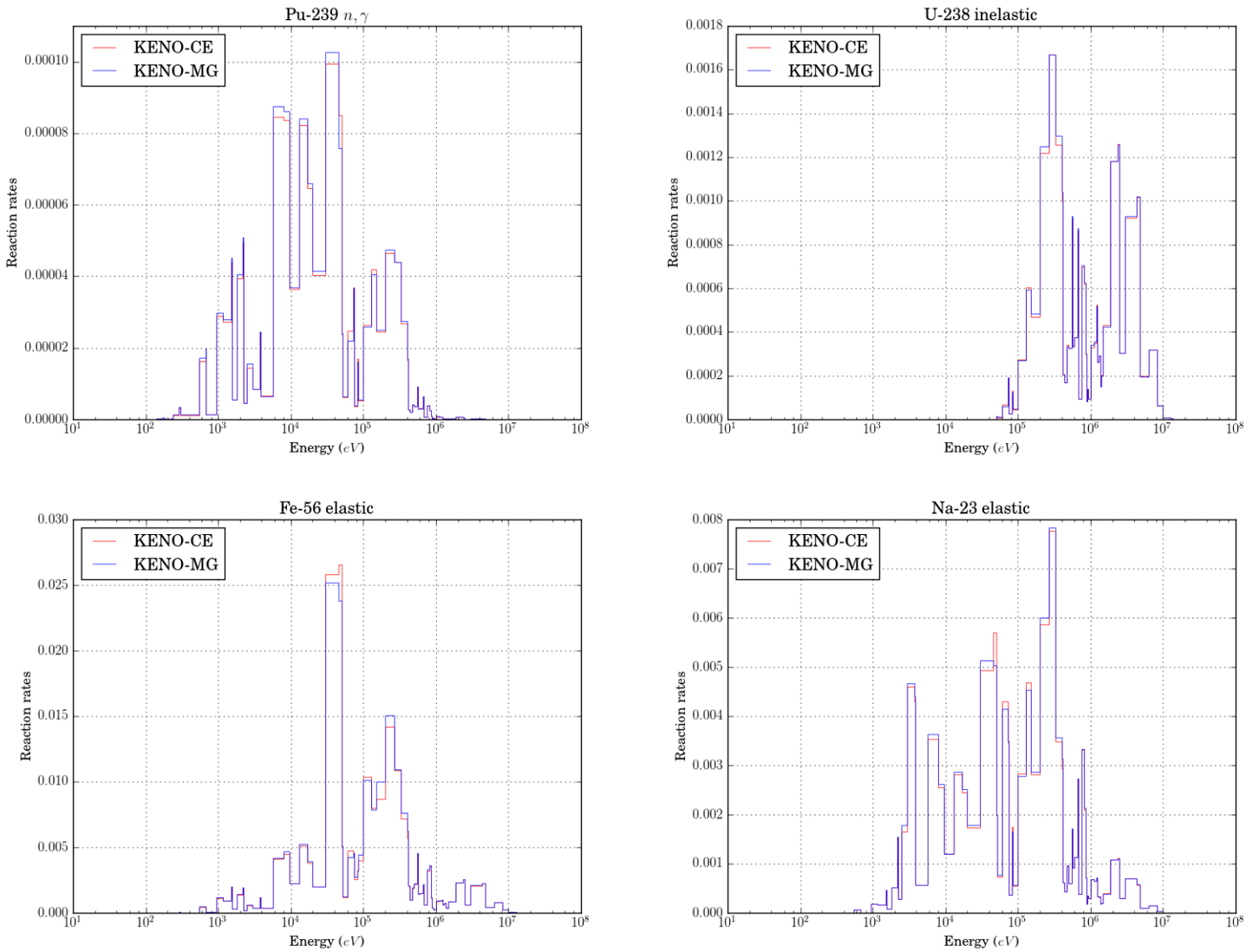

Figure 5.8: Neutron capture of Pu-239, inelastic scattering of U-238, elastic scattering of Fe-56 and elastic scattering of Na-23 in the 3D pin-cell model at nominal conditions.

Burn-up step [days]	0	102.5	205	307.5	410
By default BR k_{eff} [-]	1.37195	1.36067	1.34970	1.33904	1.32855
Problem-dependent BR k_{eff} [-]	1.37198	1.36048	1.34984	1.33904	1.32857

Table 5.6: Results for 3D pin-cell burnup calculations obtained by Serpent (Standard deviation of computed values: ±5 pcm).

5.5 Serpent calculations

As reference for comparison, calculations for the same model are performed by the three-dimensional continuous-energy Monte Carlo code Serpent.

Due to the predictor-corrector algorithm followed by Serpent, it is possible to get both multiplication factor and nuclide composition at the same depletion step. Therefore, k_{eff} values performed by Serpent correspond to the subintervals defined by the user.

At first, calculations are conducted by Serpent with the default constant branching ratios (BR) which were previously calculated from energy-dependent branching ratios in the JEFF-3.1 activation (JEFF-3.1/A) file in LWR flux spectrum. Taking into account this consideration, Table 5.6 provides the multiplication factor values along the depletion cycle. Statistical errors of the Serpent Monte Carlo solutions are lower than 5 pcm

However, it is also possible to perform the calculations with the problem-dependent branching ratios (see Table 5.6). For this purpose, an isomeric branching data library which contains energy-dependent branching ratios can be used via *set bralib* option. In this case, the employed library is the energy-dependent branching data (FILE 9) from JEFF-3.1/A library.

Therefore, problem-dependent branching ratios can be extracted from calculations using standard detectors that provide the branching ratios from initial nuclide to ground and metastable states of the new nuclide. A post-processing script is used to obtain these branching ratios.

Then, by comparing multiplication factors no relevant differences (a few pcm) can be encountered between both Serpent calculations. Thus, default branching ratios treatment followed by Serpent have not appreciable effect over k_{eff} values along the burnup cycle.

Nevertheless, problem-dependent branching ratios present significant differences regarding the default ones (Table 5.7). Thus, an optimized treatment of them can be accomplished via the *set isobra* option which allows the user to define the ratios.

By using the problem-dependent branching ratios, differences regarding nuclides densities can be observed. Nuclides from Am-241 (i.e. Am-242g and Am-242m) and Am-243

	Problem-dependent branching ratios	Serpent default branching ratios	Relative deviation [%]
Am-241→Am-242	0.91572	0.9190	-0.36%
Am-241→Am-242m	0.08428	0.0810	4.05%
Am-243→Am-244	0.06695	0.0626	6.95%
Am-243→Am-244m	0.93305	0.9374	-0.46%
Ag-109→Ag-110	0.95142	0.9540	-0.27%
Ag-109→Ag-110m	0.04858	0.0460	5.61%

Table 5.7: Relative deviation between problem-dependent and default branching ratios for capture used by Serpent.

(i.e. Am-244g and Am-244m) show relevant differences along the burnup cycle. As can be seen in Table 5.7, there are significative relative deviations between problem-dependent and default branching ratios for some capture reactions. These deviations lead to differences of about 6% and 4% for Am-244 and Am-242m densities respectively.

In conclusion, calculations performed by Serpent include an energy-dependent branching ratio treatment based on the JEFF-3.1/A data library.

5.6 SCALE and Serpent results comparison

Once calculations have been performed, the objective is to analyse possible deviations between TRITON-CE and Serpent results. Several work have been carried out on comparing SCALE and Serpent performances, mainly via criticality calculations [12] [21].

In this case, evolution of k_{eff} values along the burnup cycle as well as nuclide densities can be compared. Related to multiplication factor, Figure 5.9 shows its evolution along the burnup cycle for the pin-cell model.

At the initial time step, when any inventory calculation has not performed yet, a difference of 687 pcm is revealed between both codes. This deviation is much higher than the statistical errors presented in each Monte Carlo calculation. As it can be seen, the difference remains practically constant along the depletion cycle and at the end of the cycle the deviation is about 500 pcm.

Deviations between multiplication factors performed by KENO-VI and Serpent have been encountered previously [13]. Firstly, these differences are suggested to be the results of the application of cross section libraries that are prepared via different nuclear data processing systems; AMPX for KENO-VI and NJOY for Serpent. Moreover, there are

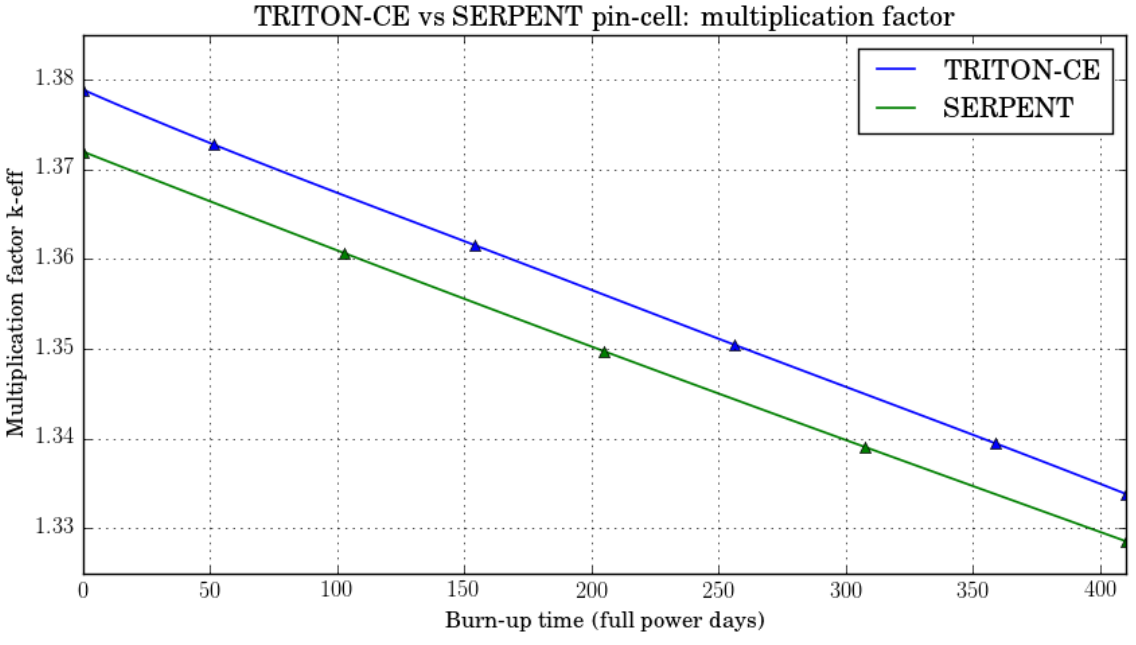

Figure 5.9: Comparison of k_{eff} evolution along the depletion cycle for the pin-cell model.

also differences in the applied probability tables for resonances in the unresolved energy range. Nevertheless, there is a low impact of the different probability tables on the neutron flux distribution; Figure 5.10 shows a very good agreement between the neutron flux distributions performed by KENO-CE and by Serpent. Note that, in this case, no differences can be attributed to the temperature interpolation of cross sections that SCALE performs for unavailable data.

Therefore, by comparing with other simplified models, the obtained results seem consistent. For the 3D pin-cell model and at the initial timestep, a reactivity difference of 364 pcm is obtained while a difference of 451 pcm results for a SFR sub-assembly based on MOX fuel [13]. It can be concluded that, for this kind of problems, Serpent provides generally a lower k_{eff} value working with the same nuclear data library.

In this sense, an in-depth analysis has been carried out in order to discover the sources of the discrepancies between both codes. By using the SFR pin-cell model, calculations have been conducted to determine the one-group microscopic cross sections of main reactions.

Table 5.8 shows the KENO-VI results and also the Serpent ones. While negligible differences have been observed for the neutron flux distribution, some deviations can be observed in this case. Taking into account the encountered relative deviations, Pu-239 and Pu-241 are the main contributors to the disagreement between both codes.

Pu-239 and Pu-241 production and capture microscopic cross sections have been col-

KENO-VI (ENDF/B-VII.1)								
1-g XS [barn]	U-235	U-238	Pu-238	Pu-239	Pu-240	Pu-241	Pu-242	Am-241
1-g fission	1.7336	0.0538	1.0942	1.7155	0.4128	2.3356	0.3066	0.3138
1-g production	4.2845	0.1490	3.3356	5.0766	1.2667	6.9500	0.9606	1.0663
1-g capture	0.4626	0.2433	0.5331	0.3835	0.4193	0.3566	0.3541	1.6012
Serpent (ENDF/B-VII.1)								
1-g XS [barn]	U-235	U-238	Pu-238	Pu-239	Pu-240	Pu-241	Pu-242	Am-241
1-g fission	1.7371	0.0539	1.0956	1.7093	0.4126	2.2903	0.3066	0.3140
1-g production	4.2933	0.1492	3.3399	5.0587	1.2661	6.8165	0.9606	1.0671
1-g capture	0.4643	0.2451	0.5363	0.3872	0.4195	0.3707	0.3518	1.6053
KENO-VI vs. Serpent: relative deviation								
	U-235	U-238	Pu-238	Pu-239	Pu-240	Pu-241	Pu-242	Am-241
1-g fission	-0.21%	-0.10%	-0.13%	0.36%	0.05%	1.98%	0.00%	-0.08%
1-g production	-0.20%	-0.11%	-0.13%	0.35%	0.04%	1.96%	-0.01%	-0.08%
1-g capture	-0.38%	-0.72%	-0.60%	-0.95%	-0.06%	-3.81%	0.64%	-0.25%

Table 5.8: Collapsed one-group microscopic cross sections performed by KENO-VI and by Serpent for SFR pin-cell model.

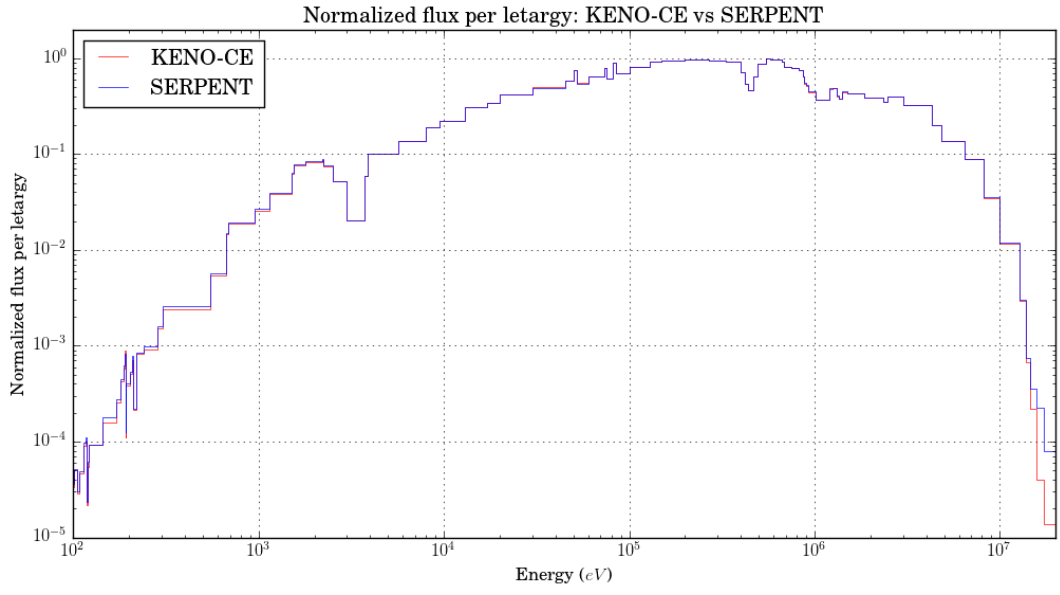

Figure 5.10: Normalized total neutron flux distribution for the pin-cell model performed by KENO-CE and by Serpent at BOL; the results are collapsed into the SCALE 252-group structure.

lapsed into SCALE-252g structure. Then, it is possible to computed the relative deviation between KENO and Serpent by using this structure. Results are plotted in Figures 5.11 and 5.12.

It can be clearly seen a very chaotic behavior in unresolved resonance range of Pu-239 and Pu-241, whose boundaries are also marked in the figure. In fact, it seems that KENO overstimates the production and understimates the capture microscopic cross sections. In contrast to this behavior, differences are negligible outside this range. Then, the different treatment of the unresolved range leads to large differences in multiplication factor between both codes. This fact is in agreement with the sensitivity analysis of the problem. The following isotope-reaction pairs are the major contributors to changes in k_{eff}: Pu-239 $\bar{\nu}$ and fission, U-238 capture, $\bar{\nu}$ and inelastic, Pu-241 $\bar{\nu}$ and fission, O-16 elastic, Pu-240 $\bar{\nu}$ and U-238 fission.

In order to complete this afirmation, two new calculations have been performed by switching off the consideration of probability tables (p-tables) during the neutron tracking. Both KENO and Serpent allow this possibility via *ptb* logical parameter in KENO and via *ures* card in Serpent. Table 5.9 summarises multiplication factors for the reference cases and for the new cases.

KENO-VI, operating with p-tables disabled, provides results very close to those of Serpent. On the other hand, the effect of p-tables in unresolved resonance range in KENO is much more stronger than in Serpent. Thus, two reasons can be responsible

Code	P-Tables in the URR	k_{eff} [-]	Δk_{eff} [pcm]
Serpent	YES	1.37202	ref
KENO-VI	YES	1.37880	-678
Serpent	NO	1.37208	-6
KENO-VI	NO	1.37211	-9

Table 5.9: Effect of using probability tables in unresolved resonance range (Standard deviation of computed values: ±4 pcm).

of that, a) the processing of ENDF nuclear data library or b) the methods inherent to each code: random number generation routines, approximations in techniques for scoring neutron multiplication or the probability table sampling method embebbed into MC code routines.

Moreover, Figures 5.11 and 5.12 also include the deviations between KENO with p-tables treatment switched off and Serpent. It can be seen clearly a very much better agreement between the codes in this new case. Note that the strange behavior presented for low energies is due to the higher statistical error in ranges where no many reactions are taking place given the neutron flux spectrum.

As future work, it is mandatory to identify an integral benchmark via ICSBEP (i.e. International Criticality Safety Benchmark Evaluation Project) that can be used to validate neutronics calculations.

Turning to the burnup calculations and related to nuclide densities evolution, Table 5.10 shows the relative deviations between nuclides densities obtained by TRITON-CE and by Serpent (Equation 5.2) in each depletion step.

$$Relative\,deviation\,(\%) = \frac{TRITON/CE - SERPENT}{SERPENT} \cdot 100 \tag{5.2}$$

As can be seen from the results, a very good agreement is observed for actinides U, Np and Pu along the burnup cycle including 60-days decay step.

On the other hand, larges bandwidths can be observed for some isotopes of the minor actinides Am and Cm. Metastable state of Am-242 presents very large deviations that can be attributed to different branching ratios treatment (Figure 5.13) followed by each code.

Another deviations can be noted. Am-242 presents a remarkable difference at the end of the decay step that is related to the decay of Am-242m to the ground state. The Am-242 will have disappeared due to its half-life value compared to the length of the

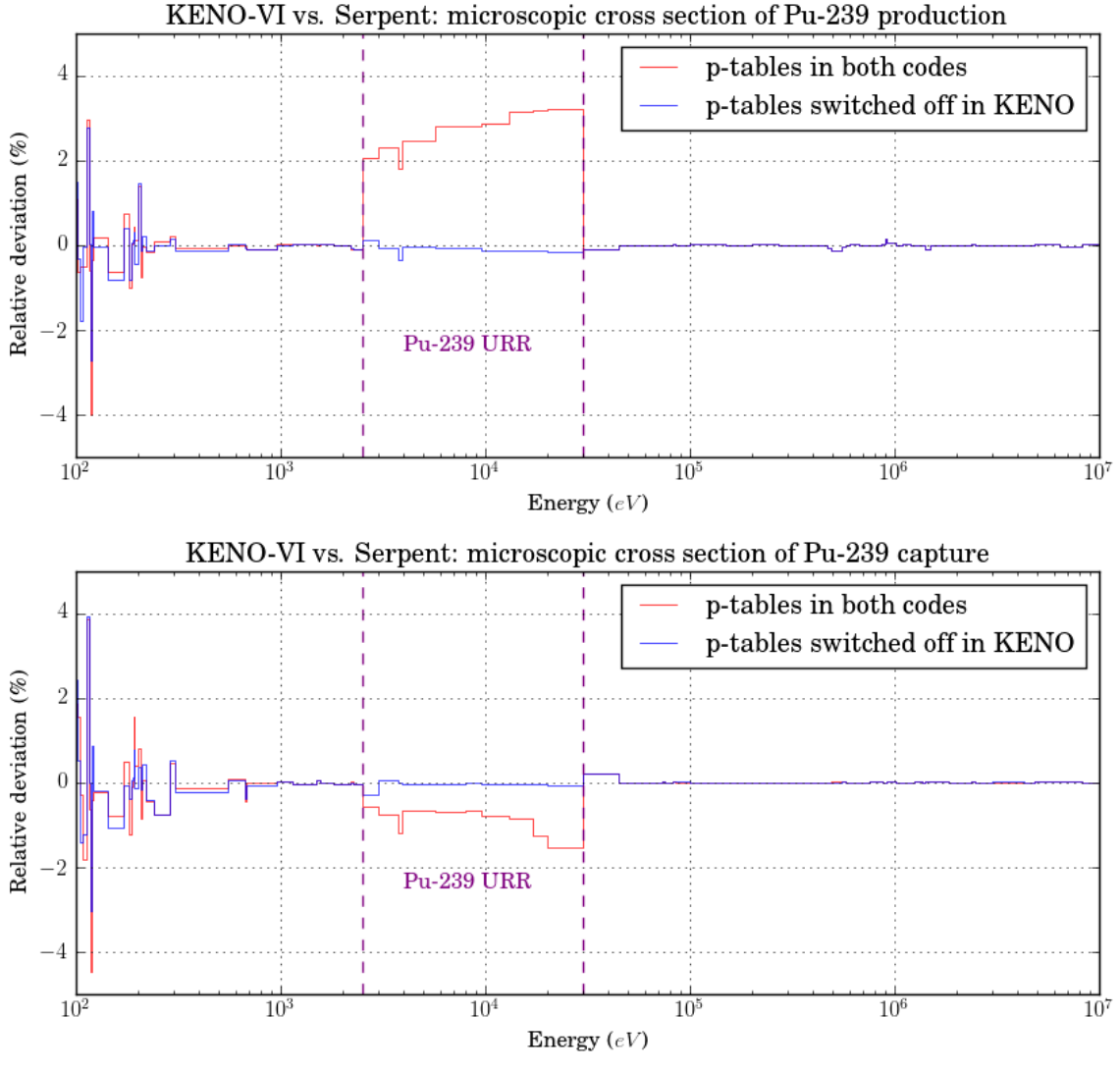

Figure 5.11: Relative deviations between KENO-VI and Serpent for Pu-239 production and capture microscopic cross sections.

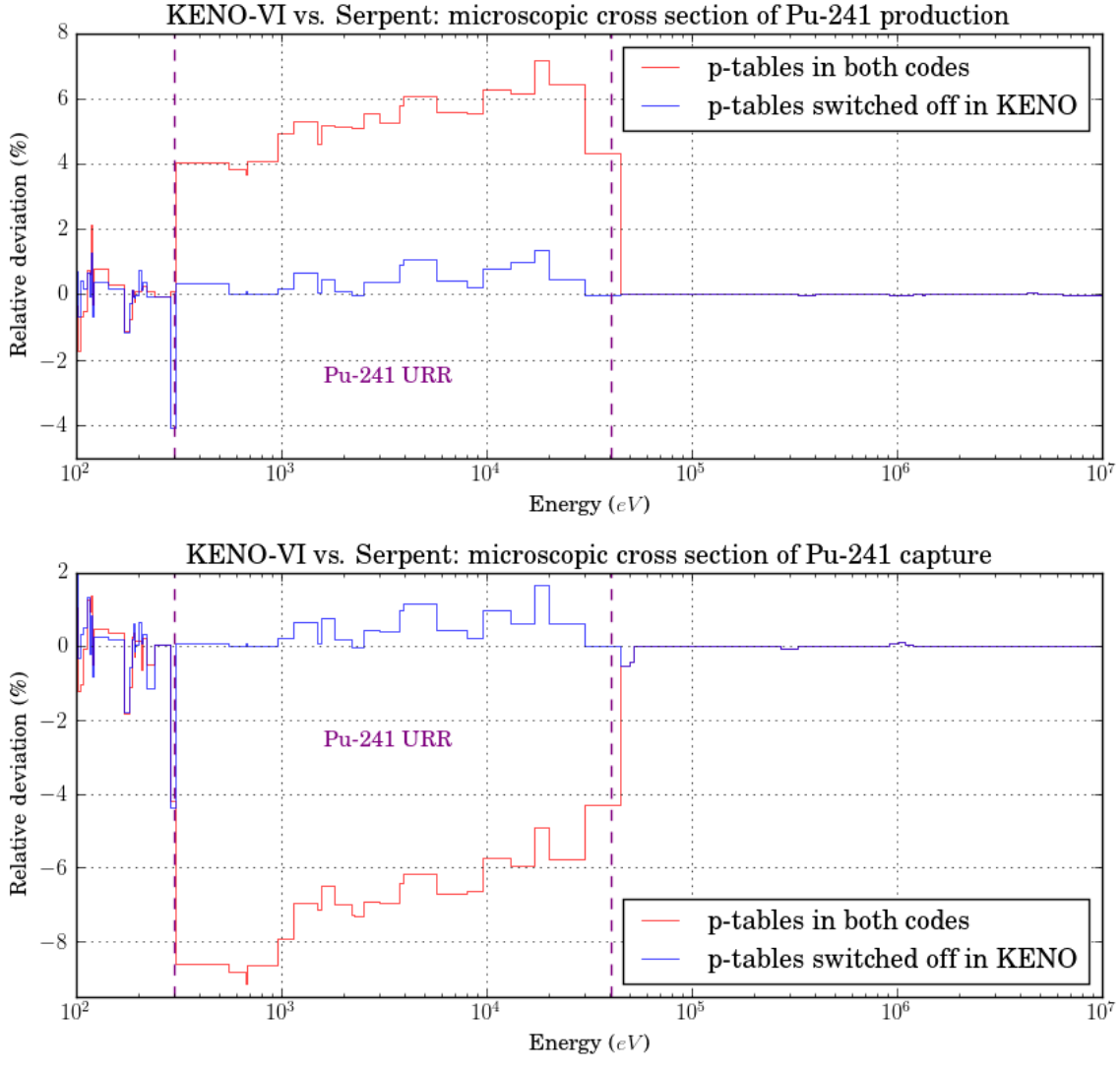

Figure 5.12: Relative deviations between KENO-VI and Serpent for Pu-241 production and capture microscopic cross sections.

Burn-up step [days]	0	102.5	205	307.5	410	470
U-234	0.00%	-0.02%	-0.06%	-0.10%	-0.14%	-0.16%
U-235	0.00%	-0.04%	-0.08%	-0.12%	-0.16%	-0.16%
U-238	0.00%	0.00%	-0.01%	-0.01%	-0.02%	-0.02%
Np-237	0.00%	0.83%	0.90%	0.82%	0.75%	0.75%
Pu-238	0.00%	-0.04%	-0.10%	-0.16%	-0.25%	-0.27%
Pu-239	0.00%	-0.03%	-0.07%	-0.10%	-0.13%	-0.13%
Pu-241	0.00%	-0.07%	-0.14%	-0.21%	-0.28%	-0.28%
Pu-242	0.00%	-0.03%	-0.07%	-0.11%	-0.14%	-0.14%
Am-241	0.00%	-0.04%	-0.07%	-0.12%	-0.16%	-0.16%
Am-242	0.00%	-6.31%	-6.39%	-6.41%	-6.46%	87.23%
Am-242m	0.00%	88.13%	87.90%	87.51%	87.22%	87.23%
Am-243	0.00%	2.04%	1.99%	1.96%	1.92%	1.93%
Am-244	0.00%	5.32%	4.91%	4.78%	4.69%	-
Am-244m	0.00%	5.52%	5.40%	5.37%	5.32%	-
Cm-243	0.00%	-5.19%	-5.61%	-5.78%	-5.88%	-5.88%
Cm-244	0.00%	5.25%	5.00%	4.91%	4.85%	4.85%
Cm-245	0.00%	6.20%	5.97%	5.88%	5.81%	5.81%
Cm-246	0.00%	7.60%	7.29%	7.18%	7.10%	7.11%
Ag-109	0.00%	4.55%	4.52%	4.48%	4.45%	4.45%
Sb-125	0.00%	-27.12%	-26.97%	-26.95%	-26.96%	-26.86%
Pm-148	0.00%	4.66%	4.65%	4.65%	4.58%	4.24%
Pm-148m	0.00%	4.13%	4.26%	4.28%	4.23%	4.23%

Table 5.10: Relative deviation of nuclides densities obtained by TRITON-CE and by Serpent for the pin-cell model.

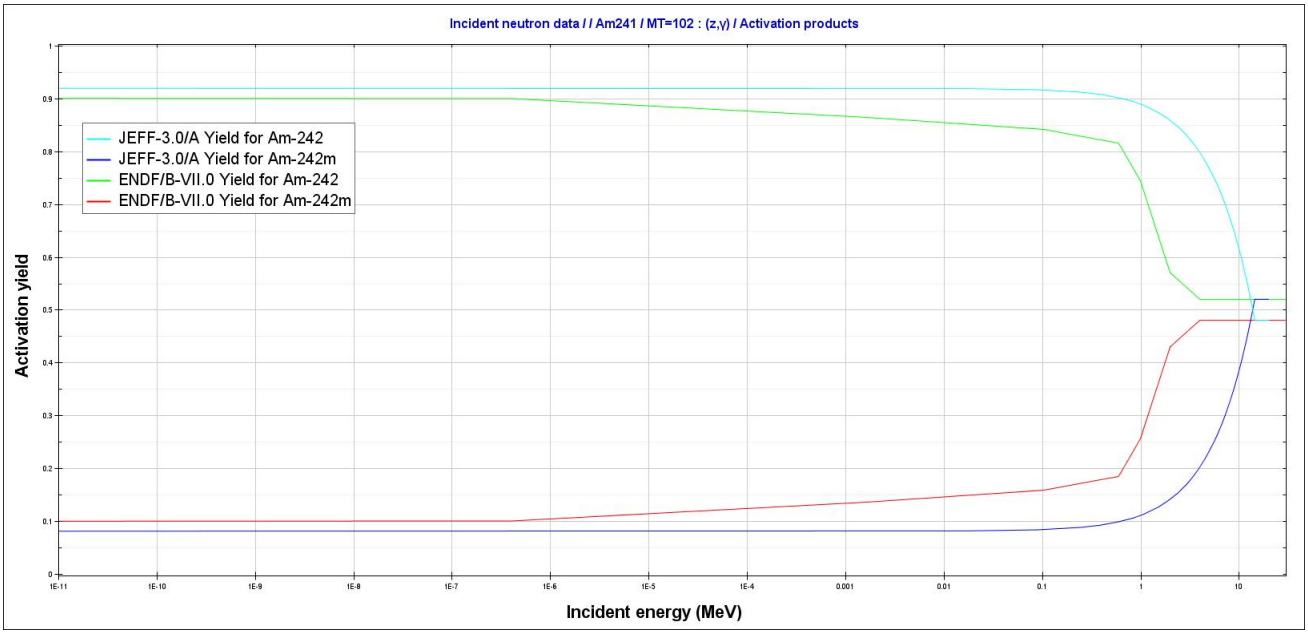

Figure 5.13: JEFF-3.0/A and ENDF/B-VII.0 Am-241 to Am-242g/m branching ratios consideration.

decay step and only the quantity produced by Am-242m decay will remain. In addition, considerable differences can be observed for the Cm inventory and they can be assigned to previous deviations for Am-242, the main precursor of the Cm isotopes.

Moreover, some fission products such as Ag, Sb or Pm present remarkable deviations. As explained in Chapter 4, ORIGEN and Serpent do not work with the same library for fission yield data. ORIGEN performs its inventory calculation based on the ENDF/B-VII.0 while Serpent uses the ENDF/B-VII.1 nuclear data library. Thus, some bandwidths for fission products densities are expected along the burnup cycle.

Taking into account that both codes uses the same nuclear data library for decay (ENDF/B-VII.1), no relevant deviations are expected in this sense and results confirm that.

Finally, Table 5.11 shows the computational resources required by each case performed in this Chapter. As can be noted, Monte Carlo burnup calculations conducted by SCALE/TRITON with continuous energy treatment require higher computational effort with respect to Serpent. Serpent was initially originated for reactor physics calculations and incorporates an optimized tracking routine that reduces considerably the calculation time.

It may be possible to reproduce SCALE-CE results using an optimized MG library for fast spectrum calculations. Then, to carry out burnup calculation based on SCALE/TRITON

	SCALE - MG	SCALE - CE	Serpent
Computational resources		48 cores 2.6 GHz 256 GB RAM	
Computational requirements	parallel 40 cores 2.1 GB RAM	parallel 40 cores 114 MB RAM	parallel 20 cores 12 GB RAM
Calculation time of a single burnup step	~0.44 h	~26.25 h	~1.6 h
Total calculation time	~2.5 h	~142 h	~14 h

Table 5.11: Computational performances for pin-cell calculations.

with similar computational requirements than Serpent, a SFR-optimized multigroup library is required.

Nevertheless, SCALE/TRITON continuous energy calculations have been performed satisfactorily, with a reasonable agreement with results obtained by Serpent. Then, the next step is to apply this methodology to the ASTRID 3D whole-core model.

Chapter 6

ASTRID full core Monte Carlo burnup calculations

6.1 Introduction

Taking into account the conclusions extracted from the 3D pin-cell model calculations, in this case the goal is to perform the Monte Carlo burnup calculations for the ASTRID 3D whole-core model (Chapter 3).

Related to depletion scheme, the 410-days cycle divided into 4 sub-intervals with the 60-days decay step is also used for the whole-core model. In this case, SCALE/TRITON deplete-by-power and deplete-by-flux modes can be assessed for different materials. Results of different modes are studied with the aim of identifying the closest ones to Serpent results.

6.2 SCALE/TRITON calculations

Though SCALE MG libraries do not work well for fast neutron spectrum, as analyzed in the previous Chapter, these libraries are also used for full core calculation. Regarding multiplication factor, the MG libraries behaviour will not be different for whole-core model but their adaptation for each core zone can be assessed via neutron flux spectrums.

6.2.1 MG calculations

Based on ENDF/B-VII.1 nuclear data library for neutron transport calculation and on the depletion scheme already used, calculation with two MG structures are performed for full core. In this case, deplete-by-flux mode is selected for fertile materials (i.e. UOX-IB and UOX-LB) while deplete-by-power mode is selected for fissile materials (i.e. MOX-IZ and MOX-OZ).

Table 6.1 collects the multiplication factor evolution performed by TRITON with 56-group and 252-group libraries. Multiplication factor statistical errors associated with Monte Carlo calculations are about 10 pcm in both cases.

As it can be observed, calculations lead to a multigroup bias of about 260 pcm at the initial time step. This deviation is reduced along the depletion scheme and at final time steps the differences is practically negligible.

It is clear that for the full core model, the 56-group structure is not well-adjusted to the fast spectrum. Spectrum detail is missed by using this structure, optimized for LWR calculations.

Related to nuclide densities, relevant bandwidths appear in some actinides such as Pu-241, Am and Cm. Therefore, the 56-group library is not very appropriate for fast spectrum calculations.

6.2.2 CE calculations

By applying the continuous energy treatment more accurate calculations will be performed by SCALE/TRITON and this is the final goal.

ASTRID whole-core model preserves the temperatures at nominal conditions. Note that KENO generates the problem-dependent cross sections by logarithmic interpolation from available temperatures. Therefore, possible deviations with Serpent calculation may be result of this temperature interpolation.

Focusing on the burnup calculations and based on the ENDF/B-VII.1 library, two different depletion modes are applied to CE calculations:

- On one hand, deplete-by-power mode is selected for the fissile material while deplete-by-flux mode is the selected one for the fertile materials. Table 6.1 collects the multiplication factor evolution using this mode (see CE mode 1).
- On the other hand, deplete-by-power mode is selected for fissile and fertile materials. In this sense, multiplication factor evolution is slightly different than the previous case (see Table 6.1 and CE mode 2).

No relevant discrepancy is observed between these two cases showing a deviation of the order of 220 pcm at the end of the burnup cycle. In fact, significant differences between the two depletion modes would indicate that the TRITON depletion subintervals are too large. Nevertheless, a detailed comparison with respect to Serpent will be carried out concerning nuclide densities.

Related to neutron flux spectrum, Figure 6.1 depicts the spectrums performed by TRITON-CE for fissile and fertile materials included in the inner core zone. As it can be observed, the upper MOX fuel presents the higher neutron flux but U-238 resonances at

Burn-up step [days]	0	51.25	153.75	256.25	358.75	410
56-group k_{eff} [-]	1.05830	1.05310	1.04477	1.03725	1.03050	1.02713
252-group k_{eff} [-]	1.05565	1.05071	1.04333	1.036487	1.03015	1.02698
CE mode 1 k_{eff} [-]	1.05004	1.04505	1.03836	1.03171	1.02574	1.02276
CE mode 2 k_{eff} [-]	1.05004	1.04478	1.03739	1.02998	1.02351	1.02028

Table 6.1: Results for full core burnup calculations performed by SCALE/TRITON-MG and by SCALE/TRITON-CE; Mode 1: deplete-by-power mode for fissile materials and deplete-by-flux mode for fertile materials, Mode 2: deplete-by-power mode for all materials (Standard deviation of computed values: ±10 pcm for MG and ±14 pcm for CE).

low energies lead to a more important flux in the UOX-IB located between both MOX zones.

6.2.3 MG effect assessment

As explained previously, the 252-group library includes several enhancements with respect to the widely-used SCALE 238-group library. However, the first one does not work very well for fast neutron spectrums calculations, as demonstrated in the previous Chapter.

For full core calculations, this trend is also confirmed via multiplication factor evolution compared to continuous energy results (see Figure 6.2). As it can be observed, the 252-group results show differences of about 560 pcm with the CE-mode1 ones at the initial timestep. This deviation decreases to 440 pcm at the end of the cycle, where 56 and 252-group results are in a good agreement.

As it can be expected, no substantial bandwidths are found by comparing the nuclide densities at the cumulative burnup steps. These differences are related to deviations of flux spectrums that KENO-VI provides to ORIGEN in each time step.

Flux spectrums performed by KENO-VI for MOX-IZ and UOX-IB materials included in the inner core zone are showed in Figure 6.3. It can be seen the disagreement between 252-group and CE distributions. The clearest differences are observed at medium-energies of the spectrum, mainly due to capture cross section of U-238.

Flux distributions for the outer core zone materials can be seen in Figure 6.4. It is clear the role that the MOX-OX material plays in this core zone respect to UOX-LB. Once again, the 252-group library does not collect the sufficient detail for the medium-energy zone of the spectrum.

Hence, SCALE MG libraries do not provide a good resolution of the resonances in the fast energy range where Sodium-cooled Fast Reactors works.

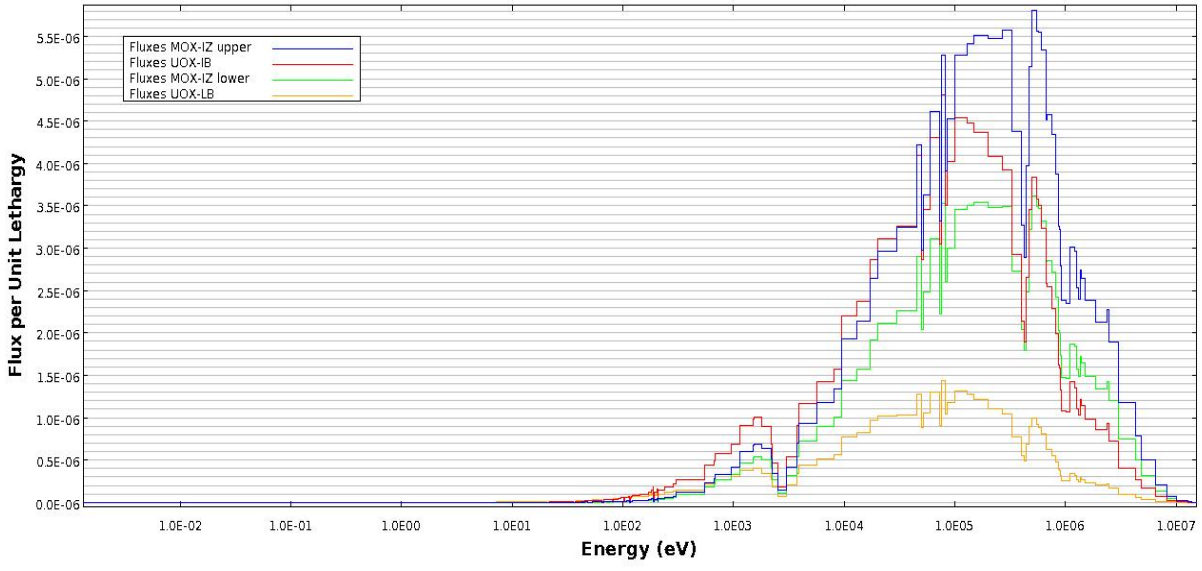

Figure 6.1: Neutron flux spectrums performed by TRITON-CE for fissile and fertile materials included in the inner core.

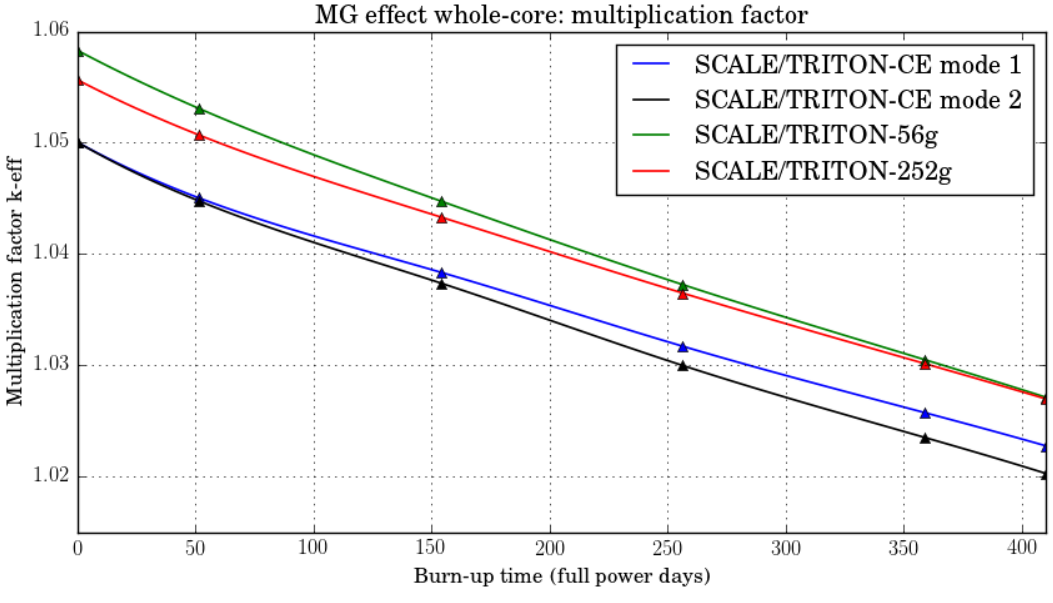

Figure 6.2: Comparison of k_{eff} evolution obtained by TRITON-MG libraries and by TRITON-CE for the full core model; Mode 1: deplete-by-power mode for fissile materials and deplete-by-flux mode for fertile materials, Mode 2: deplete-by-power mode for all materials.

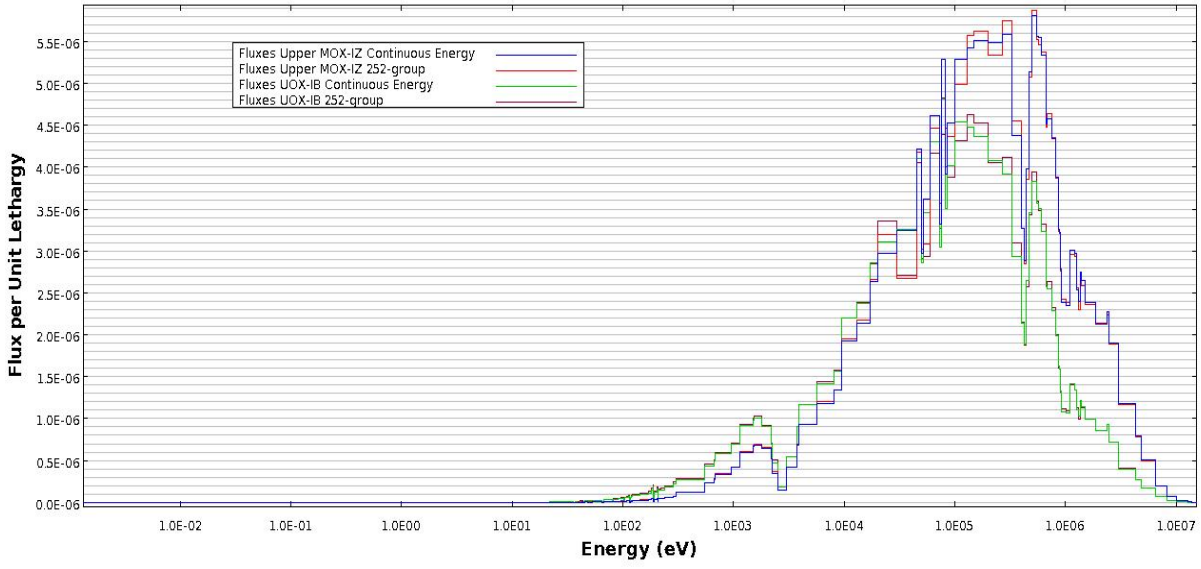

Figure 6.3: Neutron flux spectrums obtained by TRITON-252g and by TRITON-CE for the inner zone materials.

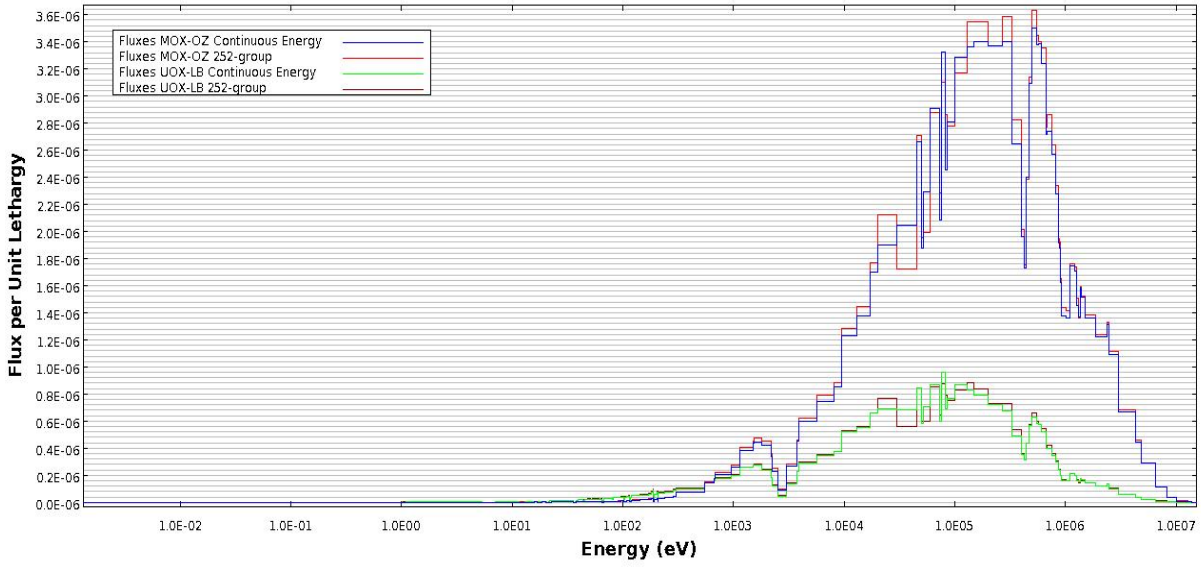

Figure 6.4: Neutron flux spectrums obtained by TRITON-252g and by TRITON-CE for the outer zone materials.

Burn-up step [days]	0	102.5	205	307.5	410
k_{eff} [-]	1.04411	1.03669	1.03053	1.02436	1.01866
k_{eff} standard deviation [pcm]	±13	±12	±13	±11	±12

Table 6.2: Results for full core burnup calculations with Serpent.

6.3 Serpent calculations

In a similar way than pin-cell case, results provided by Serpent are used as reference for comparison with TRITON-CE. Neutron transport calculations are performed using the same ENDF/B-VII.1 nuclear data library.

It is important to note that Serpent performs the burnup calculation based on the depletion-by-power mode, thus thermal power remains unvarying along the burnup cycle.

Calculations are directly performed with the problem-dependent branching ratios generation based on the JEFF-3.1/A library. Table 6.2 collects the multiplication factor evolution along the depletion cycle performed by Serpent.

6.4 SCALE and Serpent results comparison

Firstly, a previous task is conducted in order to establish the context related to full core criticality calculations carried out by KENO-VI and Serpent.

On each transport calculation KENO-VI performs a temperature interpolation for cross section generation, mainly for fissile fuel. In order to assess possible discrepancies with respect to Serpent related with this process, a single full core transport calculation at BOL is performed by KENO-VI modifying temperatures for cross sections generation. By selecting 293K as reference temperature, interpolation is not required for any material. As a result, criticality value is $k_{eff} = 1.06565 \pm 0.00010$ under these conditions.

The single criticality calculation is also performed by Serpent with the aim of assessing the temperature interpolation conducted by KENO-VI. By setting the temperature to 293K for all materials, the multiplication factor performed by Serpent is $k_{eff} = 1.05907 \pm 0.00013$. Thus, a discrepancy of 658 pcm between both codes is obtained under these conditions.

This discrepancy is coherent with results obtained for pin-cell model (680 pcm) where temperature interpolation was not required. The origin of those deviations has been in-depth analysed in the previous chapter and they have been attributed to the unresolved resonance range treatment.

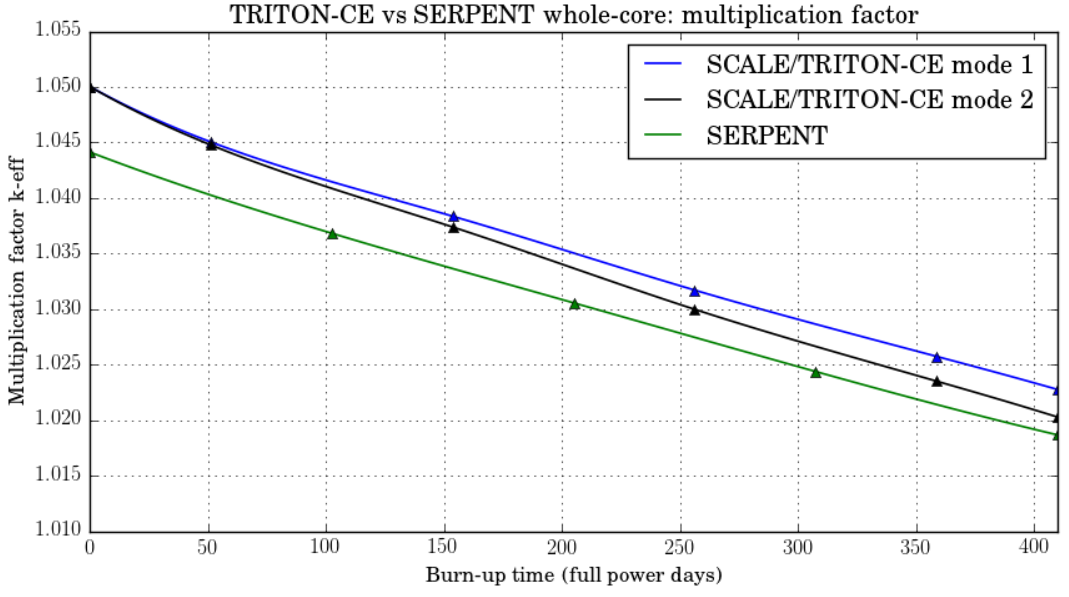

Figure 6.5: Comparison of k_{eff} evolution along the depletion cycle for the whole-core model; Mode 1: deplete-by-power mode for fissile materials and deplete-by-flux mode for fertile materials, Mode 2: deplete-by-power mode for all materials.

For burnup calculations, Tables 6.1 and 6.2 reflect a deviation of 593 pcm between TRITON-CE and Serpent at the initial time step. Thus, no significative discrepancies may be assigned to the temperature interpolation that KENO-VI performs. Then, it can be assumed that KENO results correspond to the specified temperatures.

Moreover, based on [21], a deviation of about 680 pcm is obtained using the ENDF/B-VII.0 data for ASTRID end-of-cycle criticality calculations performed by KENO-VI and Serpent. In that case, the discrepancy was partly explained by the fact that KENO-VI (SCALE 6.2beta) was not able to perform the temperature interpolation for cross section generation. Then, it may be expected a decrease of the deviation in the range of 100 pcm due to the temperature interpolation process for cross sections.

Returning to the burnup calculations, Figure 6.5 depicts multiplication factor evolution along the depletion cycle predicted by TRITON-CE in both depletion modes and by Serpent. It can be observed that TRITON-CE preserves the difference of about 500 pcm with respect to Serpent by working with depletion mode 1 which is coherent. An in-depth analysis of both depletion modes is required via nuclide concentrations evolution.

In this sense, Tables 6.3 and 6.4 collect the relative deviations of the most interesting nuclide densities ($at/b\,cm$) between both TRITON depletion modes and Serpent. In general, results are in a good agreement with the ones obtained for the pin-cell model.

While the bandwidths of the results are almost negligible, in particular actinides U

and Pu, they exhibit very considerable values for some isotopes of the minor actinides Am and Cm. Different branching ratios treatment followed by each code leads to large deviations of the metastable state of Am-242.

Related to fission products, remarkable deviations appear for some isotopes such as Sb-125. Moreover, isotopes of Ag, Sm or Gd present important bandwidths. As explained in the pin-cell case, these differences are suggested to be the result of the nuclear data library used by each code.

In addition, it can be observed that TRITON depletion mode 1 presents, in general, lower relative deviations with respect to Serpent than TRITON depletion mode 2.

For a convenient display of the results, Figure 6.6 shows the build-ups of the main isotopes (U-235, U-238, Pu-238, Pu-239 and Pu-240) as well as the relative deviations between both TRITON burnup modes and Serpent. For all the cases, TRITON burnup mode 1 presents a better agreement with Serpent than the second burnup mode. Note that for both uranium and plutonium isotopes there is a very good agreement between the codes.

In order to identify the core zones with the larger differences, a zone-wise analysis is proposed. For that, it is possible to subdivide the core into the main four zones, the inner (IZ) and the outer (OZ) MOX-based zones and the lower (LB) and inner (IB) UOX-based blankets.

Table 6.5 collects the most remarkable information concluded by this zone-wise analysis. It can be noted that MOX-based zones do not show relevant differences every cases.

On the other hand, as can be observed the UOX-based zones are the responsible of the deviations which is coherent given that the different burnup mode of the UOX. In "SCALE1", the fertile materials are depleted by following the deplete-by-flux mode while in "SCALE2" these materials are depleted by constant power in a same way for fissile materials.

Once again, it can be concluded that SCALE burnup mode 1 works in a more appropriate way taking into account its very good agreement with respect to Serpent. It was observed that this mode preserved the deviation of about 500 pcm on k_{eff} between KENO-VI and Serpent. Then, for Monte Carlo burnup calculations using SCALE-TRITON sequence, it has to be chosen the deplete-by-flux mode for fertile materials.

6.4.1 CRAM solver applied to SCALE/TRITON

As explained in Section 4.3, ORIGEN uses by default the MATREX method for solving the inventory equations. Serpent, for its part, follows the CRAM method that provides more accurate results with an higher robustness.

Nevertheless, ORIGEN can be run with the CRAM solver if the user specifies it via the *DEPLETION* data block. Then, a burnup calculation is performed using TRITON

Burn-up step [days]	0	102.5	205	307.5	410	470
U-234	0.00%	-0.00%	-0.01%	-0.03%	-0.05%	-0.08%
U-235	0.00%	0.04%	0.08%	0.12%	0.17%	0.17%
U-238	0.00%	0.00%	0.01%	0.02%	0.02%	0.02%
Np-237	0.00%	-0.62%	-0.84%	-0.76%	-0.82%	-0.81%
Pu-238	0.00%	0.00%	-0.04%	-0.10%	-0.19%	-0.25%
Pu-239	0.00%	-0.05%	-0.09%	-0.12%	-0.16%	-0.16%
Pu-241	0.00%	-0.09%	-0.17%	-0.26%	-0.34%	-0.34%
Pu-242	0.00%	-0.05%	-0.11%	-0.16%	-0.21%	-0.22%
Am-241	0.00%	0.02%	0.03%	0.04%	0.04%	-0.03%
Am-242	0.00%	-7.23%	-7.30%	-7.33%	-7.38%	82.09%
Am-242m	0.00%	82.18%	82.13%	82.11%	82.08%	82.08%
Am-243	0.00%	0.47%	0.41%	0.37%	0.34%	0.34%
Am-244	0.00%	2.18%	1.78%	1.56%	1.55%	-
Am-244m	0.00%	2.30%	2.19%	2.07%	2.10%	-
Cm-243	0.00%	-7.87%	-8.23%	-8.36%	-8.37%	-8.37%
Cm-244	0.00%	1.82%	1.60%	1.49%	1.46%	1.46%
Cm-245	0.00%	1.11%	0.81%	0.67%	0.74%	0.74%
Cm-246	0.00%	0.71%	0.41%	0.19%	0.33%	0.33%
Ag-109	0.00%	2.65%	2.60%	2.55%	2.51%	2.51%
Ag-110	0.00%	3.09%	3.11%	3.06%	3.10%	-3.19%
Sb-125	0.00%	-27.75%	-27.53%	-27.46%	-27.43%	-27.32%
Pm-147	0.00%	-0.05%	-0.07%	-0.12%	-0.17%	-0.15%

Table 6.3: Relative deviation of nuclides densities obtained by TRITON-CE (mode 1) and by Serpent for the whole-core model.

Burn-up step [days]	0	102.5	205	307.5	410	470
U-234	0.00%	-0.01%	-0.02%	-0.05%	-0.09%	-0.11%
U-235	0.00%	0.27%	0.49%	0.67%	0.82%	0.82%
U-238	0.00%	0.03%	0.06%	0.08%	0.10%	0.10%
Np-237	0.00%	-2.50%	-2.55%	-2.35%	-2.18%	-2.17%
Pu-238	0.00%	0.00%	-0.05%	-0.13%	-0.23%	-0.28%
Pu-239	0.00%	-0.28%	-0.49%	-0.65%	-0.77%	-0.78%
Pu-241	0.00%	-0.09%	-0.18%	-0.28%	-0.37%	-0.37%
Pu-242	0.00%	-0.05%	-0.11%	-0.17%	-0.22%	-0.22%
Am-241	0.00%	0.02%	0.02%	0.01%	0.00%	-0.01%
Am-242	0.00%	-7.22%	-7.15%	-7.09%	-7.08%	82.39%
Am-242m	0.00%	82.18%	82.27%	82.35%	82.39%	82.39%
Am-243	0.00%	0.50%	0.51%	0.53%	0.53%	0.53%
Am-244	0.00%	2.28%	2.02%	1.92%	1.98%	-
Am-244m	0.00%	2.41%	2.43%	2.42%	2.53%	-
Cm-243	0.00%	-7.81%	-8.06%	-8.11%	-8.08%	-8.08%
Cm-244	0.00%	1.92%	1.79%	1.76%	1.79%	1.79%
Cm-245	0.00%	1.23%	1.12%	1.00%	1.10%	1.10%
Cm-246	0.00%	0.94%	0.77%	0.58%	0.73%	0.73%
Ag-109	0.00%	2.45%	2.36%	2.29%	2.23%	2.23%
Ag-110	0.00%	2.56%	2.84%	2.69%	2.53%	-3.44%
Sb-125	0.00%	-28.05%	-27.86%	-27.80%	-27.76%	-27.66%
Pm-147	0.00%	-0.48%	-0.53%	-0.58%	-0.62%	-0.62%

Table 6.4: Relative deviation of nuclides densities obtained by TRITON-CE (mode 2) and by Serpent for the whole-core model.

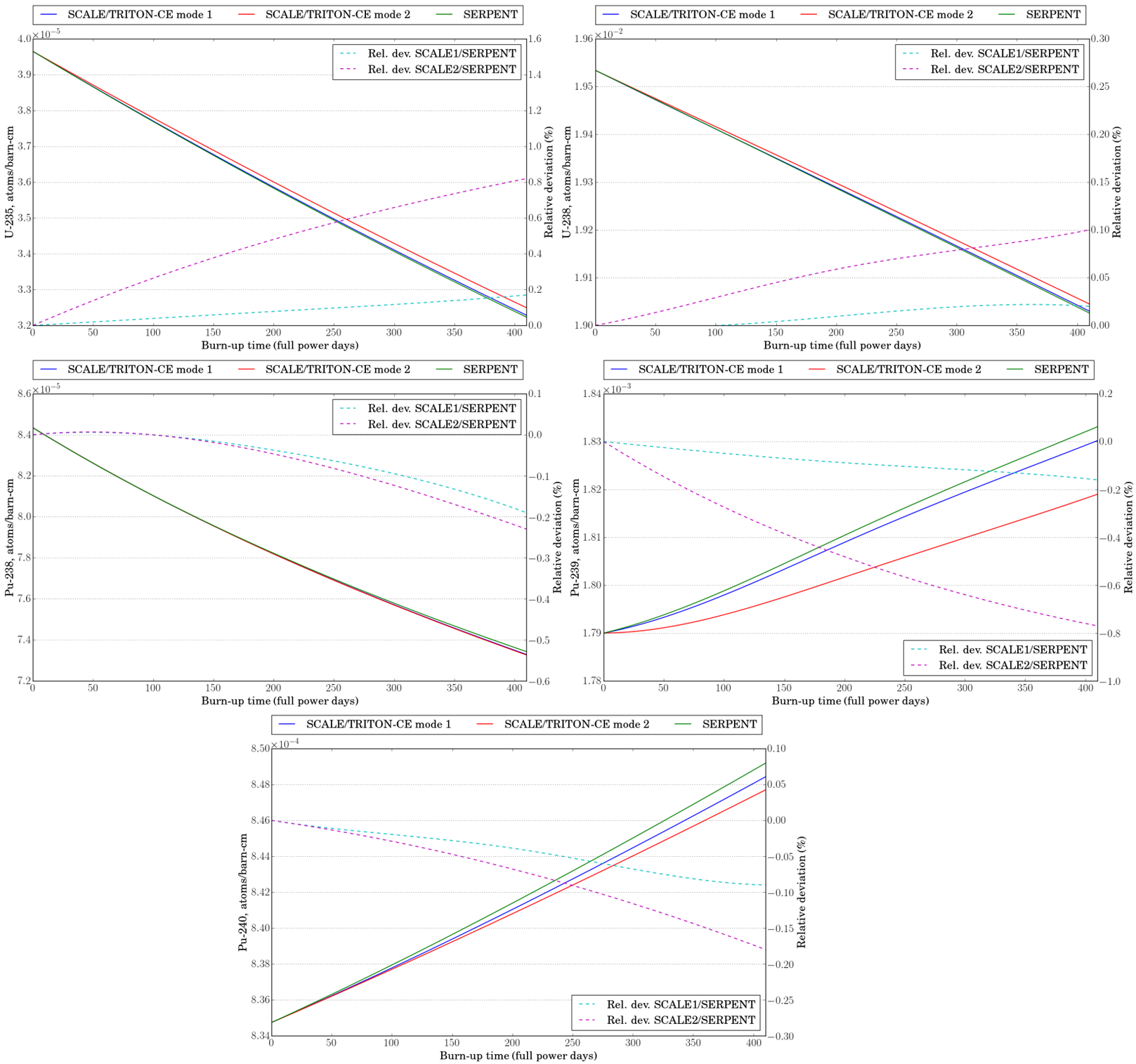

Figure 6.6: Burn-up dependencies of nuclide concentrations (U-235, U-238, Pu-238, Pu-239 and Pu-240) for the whole-core model; Mode 1: deplete-by-power mode for fissile materials and deplete-by-flux mode for fertile materials, Mode 2: deplete-by-power mode for all materials.

Burn-up step [days]		0	102.5	205	307.5	410
U-235 density relative deviation						
SCALE1 vs. SCALE2	MOX-IZ	0.00%	0.01%	0.01%	0.01%	0.00%
	MOX-OZ	0.00%	-0.01%	0.01%	0.05%	0.11%
	UOX-LB	0.00%	-0.27%	-0.51%	-0.70%	-0.88%
	UOX-IB	0.00%	-1.21%	-2.14%	-2.84%	-3.42%
SCALE1 vs. Serpent	MOX-IZ	0.00%	0.04%	0.07%	0.12%	0.13%
	MOX-OZ	0.00%	0.01%	0.03%	0.04%	0.10%
	UOX-LB	0.00%	0.04%	0.07%	0.11%	0.14%
	UOX-IB	0.00%	0.14%	0.27%	0.41%	0.50%
SCALE2 vs. Serpent	MOX-IZ	0.00%	0.03%	0.06%	0.11%	0.13%
	MOX-OZ	0.00%	0.02%	0.02%	-0.01%	-0.01%
	UOX-LB	0.00%	0.31%	0.58%	0.81%	1.03%
	UOX-IB	0.00%	1.37%	2.46%	3.34%	4.05%
Pu-239 density relative deviation						
SCALE1 vs. SCALE2	MOX-IZ	0.00%	0.00%	0.00%	0.00%	0.00%
	MOX-OZ	0.00%	0.00%	0.00%	0.01%	0.02%
	UOX-LB	-	9.63%	8.82%	8.00%	7.34%
	UOX-IB	-	16.52%	13.96%	11.82%	10.11%
SCALE1 vs. Serpent	MOX-IZ	0.00%	-0.02%	-0.04%	-0.05%	-0.08%
	MOX-OZ	0.00%	-0.02%	-0.04%	-0.06%	-0.07%
	UOX-LB	-	-0.89%	-0.84%	-0.87%	-0.90%
	UOX-IB	-	-1.63%	-1.54%	-1.52%	-1.36%
SCALE2 vs. Serpent	MOX-IZ	0.00%	-0.02%	-0.04%	-0.06%	-0.08%
	MOX-OZ	0.00%	-0.02%	-0.04%	-0.07%	-0.09%
	UOX-LB	-	-9.60%	-8.88%	-8.21%	-7.68
	UOX-IB	-	-15.57%	-13.61%	-11.92%	-10.42%

Table 6.5: Relative deviation of zone-wise U-235 and Pu-239 densities obtained by TRITON-CE (in both burnup modes) and by Serpent for the whole-core model.

Burn-up step [days]	0	51.25	153.75	256.25	358.75	410
k_{eff} [-]	1.05004	1.04510	1.03827	1.03213	1.02572	1.02225
k_{eff} statistical error [pcm]	14	14	13	13	14	-

Table 6.6: Results for full core burnup calculations with SCALE/TRITON - CE: CRAM method for solving inventory equations.

in order to assess the CRAM solver influence over the results. Runtimes required by each solver can be also assessed.

Using the deplete-by-power mode for the fissile material and deplete-by-flux mode for the fertile material, calculation based on the CRAM method provides the results collected in Table 6.6. In this case, Table 6.1 provides the reference results (MATREX method) for comparison.

No significative deviations (a few pcm) are observed with respect to multiplication factors performed by TRITON using both solvers. Moreover, a practically full agreement is obtained related to nuclide densities along the burnup cycle. Relevant actinides (i.e. U, Pu, Am and main Cm and Np isotopes) and fission products (i.e. Sr, Mo, Cs, Nd, Pm, Sm and Gd) do not present bandwidths higher than 1%.

Concerning computational times, the transport-burnup calculations using the MATREX solver requires a lower runtime (no more than 10 hours) than those in which CRAM solver is used. Note that the main restriction in this sense is the Monte Carlo neutron transport calculation.

Thus, the SCALE default solver provides high-fidelity results for depletion calculations with comparable runtimes with respect to CRAM solver that Serpent uses.

6.4.2 Computational performances

At last, computational resources required by each case performed in this Chapter are showed in Table 6.7. Once again, Monte Carlo burnup calculation conducted by SCALE/TRITON with the continuous energy treatment require a much larger computational effort than other cases.

Even though the main objective is accomplished, it is clear that computational requirements are very important. The conclusion extracted in the previous Chapter is confirmed for whole-core calculations: it is necessary a SFR-optimized multigroup library for SCALE/TRITON calculations in order to have comparable calculation times with Serpent.

Concerning calculation time spent by Serpent, note that full core case has required less time than 3D pin-cell one. It is due to required statistical error in the Monte Carlo

	SCALE - MG	SCALE - CE	Serpent
Computational resources		48 cores 2.6 GHz 256 GB RAM	
Computational requirements	parallel 40 cores 3.6 GB RAM	parallel 40 cores 144 MB RAM	parallel 20 cores 25 GB RAM
Calculation time of a single burnup step	~2.9 h	~39.1 h	~0.52 h
Total calculation time	~14.5 h	~197.8 h	~4.4 h

Table 6.7: Computational performances for full core calculations.

calculations. For pin-cell case, the statistical error was of the order of 4 pcm while for full core case, this error is about 13 pcm. The main drawback related to Serpent calculations is the required memory, very much larger than the required one by SCALE.

Chapter 7

Conclusions and future work

7.1 Conclusions

The capabilities of KENO-VI/ORIGEN coupled system from the SCALE package have been successfully assessed for full core model. The use of KENO-VI as neutron transport code avoids geometric approximations for full core calculations and allows analysis in both MG and CE modes.

It was verified that multigroup libraries provided by SCALE 6.2 (i.e. 56 and 252-group libraries) do not work very well for fast neutron spectrum calculations. Therefore, SFR-optimized MG libraries are required in order to perform burnup calculations with reasonable computational times.

Related to CE KENO-VI Monte Carlo code capabilities, no significative discrepancies may be assigned to the temperature interpolation process for cross section generation. Thus, KENO-VI is able to provide high-confidence results even if CE libraries are not available for the desired temperatures.

By comparing with Monte Carlo Serpent code, some conclusions can be extracted:

- It has been observed that KENO is predicting systematically a multiplication factor around 500-600 pcm larger than Serpent in this kind of systems by working with the same nuclear data library (ENDF/B-VII.1 in this case). Those discrepancies have been also obtained recently within the Superphénix benchmark (Task 2.1.1 of ESFR-SMART project) as well as for the optimized ESFR-SMART core calculations (Task 1.2.1).

- Deviations between KENO-VI and Serpent can be explained by the different treatment of the unresolved resonance range. It has been demonstrated that Pu-239 and Pu-241 unresolved resonance ranges are the main contributors to those deviations. Two reasons can be responsible of this behavior, on one hand the different ENDF nuclear data library processing which would entail an updating of the some cross

sections in the unresolved resonance ranges included within the library. On the other hand, it can be attributed to the methods inherent to each MC code, mainly the probability table sampling method embebbed into code routines.

- Different nuclear data libraries used by each code for radiative capture reaction ratios and fission yields lead to bandwidths for nuclide densities along the burnup cycle. Nevertheless, a good agreement was obtained for actinides uranium, plutonium and neptunium.

- No relevant deviations were encountered between the two different depletion solvers that can be used in SCALE: MATREX and CRAM.

SCALE presents as main limitation the large computational times required for Monte Carlo burnup calculations with respect to Serpent code. A number of zones reduction, that is, an homogenization of the full core model may lead to runtimes decrease. No limitations related to computational memory were found using SCALE whereas this is a drawback for Serpent calculations.

It can be concluded that SCALE6.2 would allow high-fidelity burnup calculations of Sodium-cooled Fast Reactors if CE libraries with updated data in the unresolved resonance ranges of main isotopes were provided.

7.2 Future work

A large variety of future works appear in the line followed throughout this Master Thesis. The most immediate task is the application of SCALE/TRITON methodology for Monte Carlo burnup calculations to the improved ESFR core design, which has to be developed within the ESFR-SMART during 2018.

Several future works are related to SCALE multigroup libraries generation and utilization:

- On one hand, generation of SFR-optimized MG libraries using the AMPX code is mandatory. It is expected contributions to the ESFR-SMART project with results computed with data libraries non-based on NJOY nuclear data processing code. These libraries may be very useful not only for burnup calculations but also for sensitivity and uncertainty analysis (Task 1.2.2 of the ESFR-SMART project).

- On the other hand, the optimized MG libraries may be generated with AMPX and based on JEFF-3.3 data library, released at the end of 2017. This task allows the possibility to compare results provided by using the ENDF/B-VII.1 and the JEFF-3.3 data libraries.

Moreover, the capability that KENO-VI can run in both continuous energy and multi-group will be powerful to identify the limitations of MG calculations for the improved ESFR design. Then, specific configurations and energy ranges for which an accurate resonance self-shielding still remains a challenge can be identified. This is of interest not only for the application of KENO in MG mode, but also for other MG calculation codes such as ERANOS, used by other partners within ESFR-SMART project.

In conclusion, using the AMPX processing code for MG library generation it will be possible to select the optimal MG structure and the optimal weighting spectrum.

Related to the analysis of the differences obtained between SCALE and Serpent it is required a comparison to experimental data. In this sense, an exhaustive assessment will be carried out by participating on the Task 2.1.1 of the ESFR-SMART project, "Core static neutronics and operational transients". In this task, it will be possible the validation of SCALE for SFR calculations by comparison to experimental data extracted from Supherphénix as well as an analysis of discrepancies with respect to Serpent. So far, the systematically differences obtained between SCALE and Serpent have been already encountered in this task and their origin has been explained in this work. In fact, ORNL has also reported differences around 500 pcm between KENO-VI and Shift, the new SCALE6.3 Monte Carlo code [23], for some specific fast-spectrum benchmarks [29]. It is mandatory an in-depth analysis of the origin of the discrepancies by using some fast-spectrum criticality benchmarks in ICSBEP database. As future work, it can be identified the use of SCALE/Shift computational tool instead of SCALE/KENO for simulation of SFR, including the related ESFR-SMART tasks.

As additional task, it would be interesting the development of an analysis about the propagation of statistical and nuclear data uncertainties in KENO/ORIGEN burnup calculations.

Bibliography

[1] ESFR-SMART Project Website. `http://www.esfr-smart.eu`, 2017.

[2] European Sustainable Nuclear Industrial Initiative Website. `http://http://www.snetp.eu/esnii/`, 2017.

[3] Sustainable Nuclear Energy Technology Platform. `http://www.snetp.eu`, 2017.

[4] SERPENT - a Continuous-energy Monte Carlo Reactor Physics Burnup Calculation Code. `http://montecarlo.vtt.fi`, 2018.

[5] Ana Martínez Campo. Methodologies analysis of the ASTRID-like SFR using SCALE system. Application to sodium voiding reactivity coefficients. Master's thesis, Universidad Politécnica de Madrid, 2016.

[6] Ignacio García Cruzado. Development of the 3D ASTRID core model for the Monte Carlo code KENO-VI and performance analysis. Master's thesis, Universidad Politécnica de Madrid, 2015.

[7] M. D. Dehart and S. M. Bowman. Improved radiochemical assay analyses using TRITON depletion sequences in SCALE. In *IAEA Tech. Committe Meet. on Advances in Applications of Burnup Credit to Enhance Spent Fuel Transportation, Storage, Reprocessing and Disposition*, London, UK, 2006.

[8] Nuclear Energy Division. Neutronics. Technical report, CEA, 2015.

[9] Nuclear Energy Division. Sodium-Cooled Nuclear Reactors. Technical report, CEA, 2016.

[10] B. T. Rearden et al. Monte Carlo capabilities of the SCALE code Systems. *Annals of Nuclear Energy*, 82:130–141, 2015.

[11] F. Bostelmann et al. Assessing and enhancing SCALE capabilites to model fast neutron spectrum systems. Generation of AMPX MG libraries for fast reactor systems. In *SFR-UAM-2 meeting*, Paul Scherrer Institut, Switzerland, 2016.

[12] F. Bostelmann et al. Criticality calculations of the Very High Temperature Reactor Critical Assembly benchmark with SERPENT and SCALE/KENO-VI. *Annals of Nuclear Energy*, 90:343–352, 2016.

[13] F. Bostelmann et al. SCALE Multi-Group libraries for Sodium-cooled Fast Reactor Systems. In *M&C 2017 - International Conference on Mathematics & Computational Methods Applied to Nuclear Science & Engineering*, Jeju, Korea, 2017.

[14] G. Rimpault et al. Objectives and Status of the OECD/NEA sub-group on Uncertainty Analysis in Modelling (UAM) for Design, Operation and Safety Analysis of SFRs. In *FR17 - International Conference on Fast Reactors and Related Fuel Cycles: Next Generation Nuclear Systems for Sustainable Development*, 2017.

[15] J. Rouault et al. *Handbook of Nuclear Engineering*, chapter 21: Sodium Fast Reactor Design: Fuels, Neutronics, Thermal-Hydraulics, Structural Mechanics and Safety, pages 2321–2710. Springer, 2010.

[16] J.J. Herrero et al. Nuclear data uncertainty propagation to reactivity coefficients of a Sodium Fast Reactor. *Nuclear Data Sheets*, 118:535–537, 2014.

[17] K. Mikityuk et al. ESFR-SMART: new Horizon-2020 project on SFR Safety. In *FR17 - International Conference on Fast Reactors and Related Fuel Cycles: Next Generation Nuclear Systems for Sustainable Development*, 2017.

[18] N. García-Herranz et al. Applicability of the MCNP-ACAB system to inventory prediction in high burn-up fuels: sensitivity/uncertainty estimates. In *Int. Conf. on Mathematics and Computation*, Avignon, France, 2005.

[19] N. García-Herranz et al. Nuclear data sensitivity and uncertainty assessment of sodium voiding reactivity coefficients of an ASTRID-like Sodium Fast Reactor. In *ND 2016 - International Conference on Nuclear Data for Science and Technology*, 2016.

[20] R. Ochoa et al. A comparative study of Monte Carlo-coupled depletion code applied to a Sodium Fast Reactor design loaded with Minor Actinides. *Annals of Nuclear Energy*, 57:32–40, 2013.

[21] S. Bortot et al. European benchmark on the ASTRID-like low-void-effect core characterization: neutronic parameters and safety coefficients. In *ICAPP2015 - International Congress on Advances in Nuclear Power Plants*, Nice, France, 2015.

[22] S. Maharramova et al. Comparison of HELIOS-2.1 and SCALE-6.1 codes on pin-cell model. *Annals of Nuclear Energy*, 117:155–164, 2018.

[23] T. M. Pandya et al. Implementation, capabilities, and benchmarking of Shift, a massively parallel Monte Carlo radiation transport code. *Journal of Computational Physics*, 308:239–272, 2016.

[24] A. Isotalo and P. A. Aarnio. Comparison of depletion algorithms for large systems of nuclides. *Annals of Nuclear Energy*, 38:261–268, 2011.

[25] J. Leppanen. *SERPENT - a Continuous-energy Monte Carlo Reactor Physics Burnup Calculation Code*. VTT Technical Research Centre of Finland, 2015.

[26] Raquel Ochoa. *Core physics and safety analysis of Generation-IV Sodium Fast Reactors using existing and newly developed computational tools*. PhD thesis, Universidad Politécnica de Madrid, 2013.

[27] OECD/NEA. Technology Roadmap Update for Generation IV Nuclear Energy Systems. Technical report, Generation IV International Forum, 2014.

[28] M. Pusa and J. Leppanen. Computing the matrix exponential in burnup calculations. *Journal of Nuclear Science and Technology*, 164:140–150, 2010.

[29] B. T. Rearden. Overview of SCALE Activities. In *OECD/NEA Working Party on Reactor Systems Uncertainty Analysis in Modeling*, Lucca, Italy, May 2018.

[30] B.T. Rearden and M. A. Jesse. *Scale 6.2: A Comprehensive Modeling and Simulation Suite for Nuclear Safety Analysis and Design; Includes ORIGEN and AMPX*. Oak Ridge National Laboratory, 2016.

[31] Pierre Sciora. ASTRID Core Specifications. Technical Report D6.1.1-1, CEA, 2014.

[32] W.S. Yang. Fast Reactor Physics and Computational Methods. *Nuclear Engineering and Technology*, 44(2), March 2012.